Contents

Chapter 15

Turbulence

Version 1115.1.K, 6 February 2012
Please send comments, suggestions, and errata via email to kip@caltech.edu, or on paper to Kip Thorne, 350-17 Caltech, Pasadena CA 91125

Box 15.1
Reader's Guide

- This chapter relies heavily on Chaps. 13 and 14.
- The remaining chapters on fluid mechanics and magnetohydrodynamics (Chaps. 16–18) do not rely significantly on this chapter, nor do any of the remaining chapters in this book.

15.1 Overview

In Sec. 13.7.6, we derived the Poiseuille formula for the flow of a viscous fluid down a pipe by assuming that the flow is laminar, i.e. that it has a velocity parallel to the pipe wall. We showed how balancing the stress across a cylindrical surface led to a parabolic velocity profile and a rate of flow proportional to the fourth power of the pipe diameter, d. We also defined the Reynolds number; for pipe flow it is $\mathrm{Re}_d \equiv \bar{v}d/\nu$, where $\bar{v}$ is the mean speed in the pipe. Now, it turns out experimentally that the pipe flow only remains laminar up to a critical Reynolds number that has a value in the range $\sim 10^3 - 10^5$ depending on the smoothness of the pipe's entrance and roughness of its walls. If the pressure gradient is increased further (and thence the mean speed $\bar{v}$ and Reynolds number Re_d are increased), then the velocity field in the pipe becomes irregular both temporally and spatially, a condition known as *turbulence*.

Turbulence is common in high Reynolds number flows. Much of our experience of fluids involves air or water for which the kinematic viscosities are $\sim 10^{-5}$ and 10^{-6} m^2 s^{-1} respectively. For a typical everyday flow with a characteristic speed of $v \sim 10$ m s^{-1} and a

characteristic length of $d \sim 1$m, the Reynolds number is huge: $\mathrm{Re}_d = vd/\nu \sim 10^6 - 10^7$. It is therefore not surprising that we see turbulent flows all around us. Smoke in a smokestack, a cumulus cloud and the wake of a ship are three examples.

In Sec. 15.2 we shall illustrate the phenomenology of the transition to turbulence as Re_d increases using a particularly simple example, the flow of a fluid past a circular cylinder oriented perpendicular to the line of sight. We shall see how the flow pattern is dictated by the Reynolds number and how the velocity changes from steady creeping flow at low Re_d to fully-developed turbulence at high Re_d.

What *is* turbulence? Fluid dynamicists can certainly recognize it but they have a hard time defining it precisely,[1] and an even harder time describing it quantitatively. So typically for a definition they rely on empirical, qualitative descriptions of its physical properties (Sec. 15.3). Closely related to this description is the crucial role of vorticity in driving turbulent energy from large scales to small (Sec. 15.3.1).

At first glance, a quantitative description of turbulence appears straightforward. Decompose the velocity field into Fourier components just like the electromagnetic field when analyzing electromagnetic radiation. Then recognize that the equations of fluid dynamics are nonlinear, so there will be coupling between different modes (akin to wave-wave coupling between optical modes in a nonlinear crystal, discussed in Chap. 10). Analyze that coupling perturbatively. The resulting *weak-turbulence formalism* (some of which we sketch in Secs. 15.4.1 and 15.4.2, and Ex. 15.4) is useful when the turbulence is not too strong.[2]

However, most turbulent flows come under the heading of *fully developed* or *strong turbulence*, and cannot be well described in the weak-turbulence manner. Part of the problem is that the $(\mathbf{v}\cdot\nabla)\mathbf{v}$ term in the Navier-Stokes equation is a strong nonlinearity, not a weak coupling between linear modes. As a consequence, eddies of size ℓ persist for typically no more than one turnover timescale $\sim \ell/v$ before they are broken up, and so do not behave like weakly coupled normal modes.

In the absence of a decent quantitative theory of strong turbulence, fluid dynamicists sometimes simply push the weak-turbulence formalism into the strong-turbulence regime, and use it there to gain qualitative or semi-quantitative insights (e.g. Fig. 15.7 and associated discussion in the text). A simple alternative (which we will explore in Sec. 15.4.3 in the context of wakes and jets, and in Sec. 15.5 for turbulent boundary layers) is intuitive, qualitative and semiquantitative approaches to the *physical* description of turbulence. We emphasize, the adjective physical, because our goal is not just to produce empirical descriptions of the consequences of turbulence, but rather to comprehend the underlying physical character of turbulence, going beyond purely empirical rules on one hand and uninstructive mathematical expansions on the other. This means that the reader must be prepared to settle for order-of-magnitude scaling relations based on comparing the relative magnitudes of individual terms in the governing fluid dynamical equations. At first, this will seem quite unsatisfactory. However, much contemporary physics has to proceed with this methodology. It is simply too hard, in turbulence and some other phenomena, to discover elegant mathematical counterparts to the Kepler problem or the solution of the Schrödinger equation for

[1] The analogy to Justice Potter Stewart's definition of pornography should be resisted.

[2] Another weak-turbulence formalism which is developed along similar lines is the *quasi-linear* theory of nonlinear plasma interactions, which we shall develop in Chap. 22.

the hydrogen atom.

One triumph of this approach (Sec. 15.4.4) is the Kolmogorov analysis of the shape of the time-averaged turbulent energy spectrum (the turbulent energy per unit wave number, as a function of wave number), in a stationary turbulent flow. If the turbulence extends over several octaves of wave number (as it almost always does), then scaling arguments dictate with confidence the spectrum's shape: the famous *Kolmogorov spectrum* for turbulence. This spectrum has been verified experimentally under many different conditions.

In the context of wakes and jets (Sec. 15.4.3), this simple, physical, approach to turbulence will elucidate some remarkable phenomena: voracious *entrainment* of non-turbulent ambient fluid into turbulent wakes and jets; the crucial role that large eddies play in this entrainment; the the resulting highly irregular boundaries of wakes and jets and resulting *intermittency* of their flow; and the Coanda effect, in which voracious entrainment sucks turbulent wakes and jets toward solid walls and makes them stick.

In the context of turbulent boundary layers, our physical approach will reveal semi-quantitatively the structures of such boundary layers (Sec. 15.5.1), and it will explain why turbulent boundary layers generally exert more shear stress on a surface than laminar boundary layers, but nevertheless usually produce less total drag (Sec. 15.5.2): it is because they are less prone to separation from the surface when subjected to an adverse pressure gradient (a variant of the Coanda effect). For this reason, turbulence is often induced artificially in boundary layers, e.g. those going over the top of an airplane wing, or those on one face of a ball. In Sec. 15.5.3 we shall briefly discuss how turbulence can arise through instability of a laminar boundary layer; and in Sec. 15.5.4 we shall examine some applications to balls moving through the air (golf balls, cricket balls, baseballs, ...).

Whether or not a flow becomes turbulent can have a major influence on how fast chemical reactions occur in liquids and gases; this is another motivation for artificially inducing or surpressing turbulence.

One can gain additional insight into turbulence by a technique that is often useful when struggling to understand complex physical phenomena: Replace the system being studied by a highly idealized model system that is much simpler than the original one, both conceptually and mathematically, but that retains at least one central feature of the original system. Then analyze the model system completely, with the hope that the quantitative insight so gained will be useful in understanding the original problem. This approach has been central, e.g., to research in quantum cosmology, where one tries to understand how the initial conditions for the expansion of the universe were set, and to do so one works with model universes that have only a few degrees of freedom. Similarly, since the 1970s new insights into turbulence have come from studying idealized *dynamical systems* that have very small numbers of degrees of freedom, but have the same kinds of nonlinearities as produce turbulence in fluids. We shall examine several such low-dimensional dynamical systems and the insights they give in Sec. 15.6.

The most useful of those insights deal with the onset of weak turbulence, and the fact that it seems to have much in common with the onset of *chaos* (irregular and unpredictable dynamical behavior) in a wide variety of other dynamical systems — e.g., coupled pendula, electric circuits, and planets, asteroids, satellites and rings in the solar system. A great discovery of modern classical physics/mathematics has been that there exist organizational

principles that govern the behavior of these seemingly quite different chaotic physical systems. In Sec. 15.6 we shall discuss some very simple models for the onset of chaos and shall outline the relationship of those models to the behavior of turbulent fluids.

Despite these elegant modern insights, those features of turbulence that are important in practical situations, e.g. in aeronautical or marine engineering, are still described today only qualitatively and empirically. This is an indication of how far we are from a satisfactory, physical theory of turbulence.

In parallel with studying this chapter, in order to build up physical intuition the reader is urged to watch movies and study photographs that deal with turbulence; see Box 15.2.

Box 15.2
Movies and Photographs on Turbulence

We strongly recommend that the reader view the following movies that deal with turbulence:

- *Turbulence*, by Robert W. Stewart (1968), film in the series by the National Committee for Fluid Mechanics Films, available in 2012 at `http://web.mit.edu/hml/ncfmf.html` .
- *Laminar and Turbulent Flow*, by Hunter Rouse (ca 1963), available in 2012 at `http://www.iihr.uiowa.edu/research/publications-and-media/films-by-hunter-rouse/` .

Also useful are photographs of turbulence, e.g. in Van Dyke (1982).

15.2 The Transition to Turbulence - Flow Past a Cylinder

We shall illustrate qualitatively how a flow (and especially its transition to turbulence) depends on its Reynolds number by considering a specific problem, the flow of a uniformly moving fluid past a cylinder oriented transverse to the line of sight (Fig. 15.1). We assume that the flow velocity is very small compared with the speed of sound, so the effects of compressibility can be ignored. Let the cylinder diameter be d and choose this as the characteristic length in the problem. Similarly, let the velocity far upstream be V and choose this as the characteristic velocity, so the Reynolds number is

$$\boxed{\mathrm{Re}_d = \frac{Vd}{\nu}} \,. \tag{15.1}$$

We assume, initially, that the flow is stationary (no turbulence) as well as incompressible, and the effects of gravity are negligible. Then the equations governing the flow are incompressibility,

$$\boldsymbol{\nabla} \cdot \mathbf{v} = 0 \,, \tag{15.2a}$$

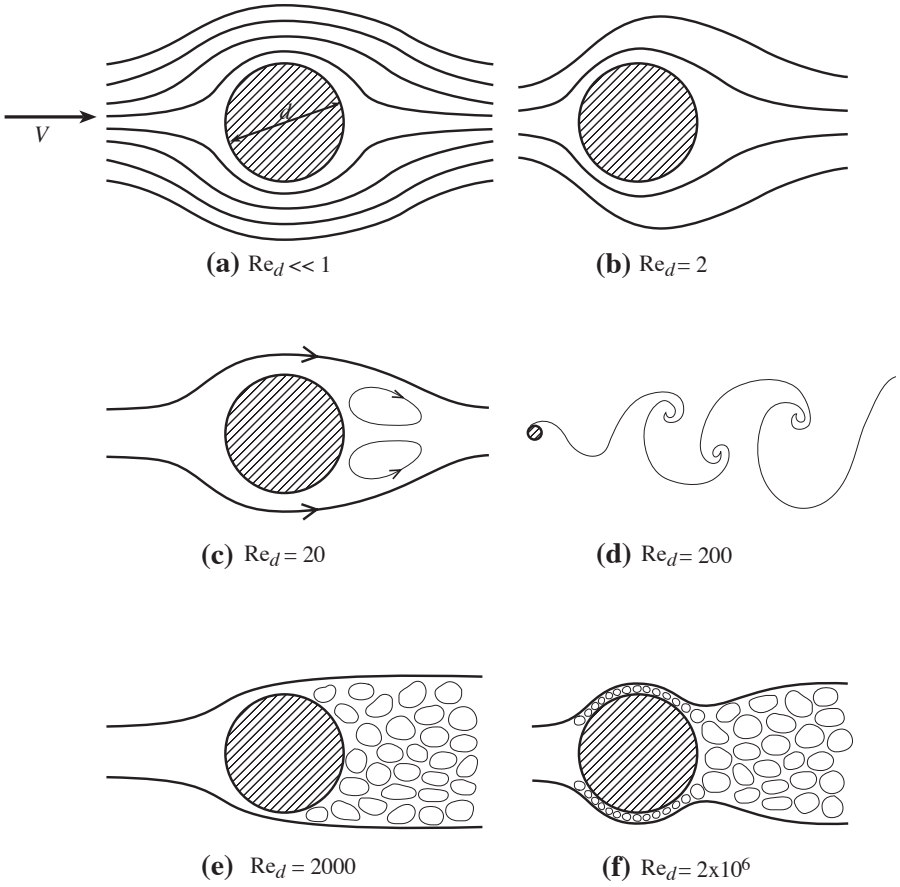

Fig. 15.1: Schematic depiction of flow past a cylinder for steadily increasing values of the Reynolds number $\mathrm{Re}_d = Vd/\nu$ as labeled. There are many photographs, drawings, and simulations of this flow on the web, perhaps best found by Googling "von Karman vortex street".

and the time-independent Navier-Stokes equation (13.65) with $\partial\mathbf{v}/\partial t = 0$:

$$\mathbf{v}\cdot\boldsymbol{\nabla}\mathbf{v} = -\frac{\boldsymbol{\nabla}P}{\rho} + \nu\nabla^2\mathbf{v}\ . \tag{15.2b}$$

These four equations (one incompressibility, three components of Navier-Stokes) can be solved for the pressure and the three components of velocity subject to the velocity vanishing on the surface of the cylinder and becoming uniform far upstream.

From the parameters of the flow (the cylinder's diameter d, the fluid's incoming velocity V and its density ρ and kinematic viscosity ν) we can construct only one dimensionless number, the Reynolds number $\mathrm{Re}_d = Vd/\nu$. (If the flow speed were high enough that incompressibility fails, then the sound speed c_s would also be a relevant parameter and there would be a second dimensionless number, the Mach number $M = V/c_s$; Chap. 17). With Re_d the only dimensionless number, we are guaranteed on dimensional grounds that the solution to the flow equations can be expressed as

$$\boxed{\mathbf{v}/V = \mathbf{U}(\mathbf{x}/d, \mathrm{Re}_d)}\ . \tag{15.3}$$

Here $\mathbf{U}$ is a dimensionless function of the dimensionless $\mathbf{x}/d$, and it can take wildly different forms depending on the value of the Reynolds number Re_d; cf. Fig. 15.1, which we shall discuss below.

The functional form (15.3) of $\mathbf{v}$ has important implications. If we compute the flow for specific values of the upstream velocity V, the cylinder's diameter d and the kinematic viscosity ν and then double V and d and quadruple ν so Re_d is unchanged, then the new solution will be similar to the original solution. It can be produced from the original by rescaling the flow velocity to the new upstream velocity and the distance to the new cylinder diameter. [For this reason, Eq. (15.3) is sometimes called a *scaling relation*.] On the other hand, if we had only doubled the kinematic viscosity, the Reynolds number would have also doubled and we could be dealing with a qualitatively different flow.

In discussing the flow past the cylinder, a useful concept is the *stagnation pressure* in the upstream flow. This is the pressure the fluid would have, according to the Bernoulli Principle $v^2/2 + u + P/\rho = \text{const}$, if it were brought to rest at the leading edge of the cylinder without significant action of viscosity. Ignoring the effects of compressibility (so u and ρ are constant), this stagnation pressure is

$$\boxed{P_{\text{stag}} = P_0 + \frac{1}{2}\,\rho V^2}\,;\,, \tag{15.4}$$

where P_0 is the upstream pressure. Suppose that this stagnation pressure were to act over the whole front face of the cylinder, while the pressure P_0 acted on the downstream face. The net force on the cylinder per unit length, F_D, would then be $\frac{1}{2}\rho V^2 d$. This is a first rough estimate for the drag force. It is conventional to define a *drag coefficient* as the ratio of the actual drag force per unit length to this rough estimate:

$$C_D \equiv \frac{F_D}{\frac{1}{2}\rho V^2 d}\,. \tag{15.5}$$

This drag coefficient, being a dimensionless feature of the flow (15.3), can depend only on the dimensionless Reynolds number Re_d: $C_D = C_D(\mathrm{Re}_d)$; see Fig. 15.2. Similarly for flow

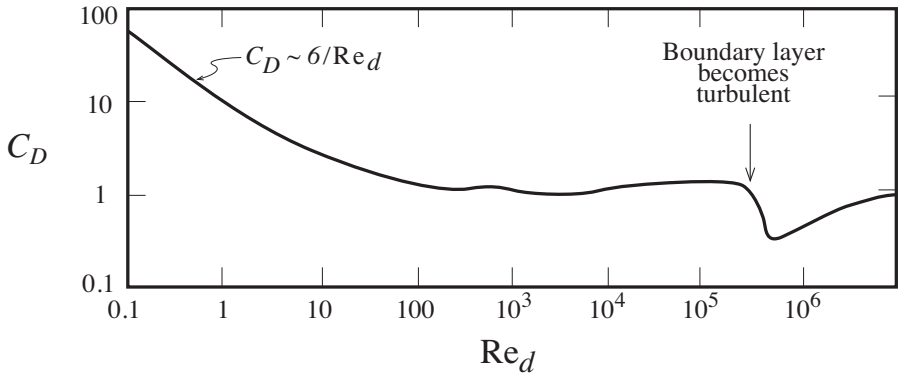

Fig. 15.2: Drag coefficient C_D for flow past a cylinder as a function of Reynolds number $\mathrm{Re}_d = Vd/\nu$. This graph, adapted from Fig. 3.14 of Tritton (1977), is based on experimental measurements.

past a body with cross sectional area A perpendicular to the flow and with any other shape, the drag coefficient

$$\boxed{C_D \equiv \frac{F_{\rm drag}}{\frac{1}{2}\rho V^2 A}} \tag{15.6}$$

will be a function only of Re. However, the specific functional form of $C_D(\mathrm{Re})$ will depend on the body's shape.

Now, turn to the details of the flow around a cylinder as described in Figs. 15.1 and 15.2. At low Reynolds number, $\mathrm{Re}_d \ll 1$, there is creeping flow (Fig. 15.1a) just like that analyzed in detail for a spherical obstacle in Sec. 14.3.2. As you might have surmised by tackling Ex. 14.6, the details of low-Reynolds-number flow past a long object such as a cylinder are subtly different from those of flow past a short one such as a sphere. This is because, for a cylinder, inertial forces become comparable with viscous and pressure forces at distances $\sim d/\mathrm{Re}_d$ where the flow is still significantly perturbed from uniform motion, while for short objects inertial forces become significant only at much larger radii, where the flow is little perturbed by the object's presence. Despite this, the flow streamlines around a cylinder at $\mathrm{Re}_d \ll 1$ are similar to those for a sphere and are approximately symmetric between upstream and downstream. The fluid is decelerated by viscous stresses as it moves past the cylinder along these streamlines and the pressure is higher on the cylinder's front face than on its back. Both effects contribute to the net drag force acting on the cylinder. The momentum removed from the flow is added to the cylinder. At cylindrical radius $\varpi \ll d/\mathrm{Re}_d$ the viscous stress dominates over the fluid's inertial stress, and the fluid momentum therefore is being transferred largely to the cylinder, at a rate per unit area $\sim \rho V^2$, while at $\varpi \gtrsim d/\mathrm{Re}_d$ the viscous and inertial stresses are comparable and balance each other, and the flow's momentum is not being transferred substantially to the cylinder. This implies that the effective cross sectional width over which the cylinder extracts the fluid momentum is $\sim d/\mathrm{Re}_d$, and correspondingly the net drag force per unit length is $F \sim \rho V^2 d/\mathrm{Re}_d$, which implies [cf. Eq. (15.5)] a drag coefficient $\sim 1/\mathrm{Re}_d$ at low Reynolds numbers $\mathrm{Re}_d \ll 1$. A more careful analysis gives $C_D \sim 6/\mathrm{Re}_d$, as shown experimentally in Fig. 15.2.

As the Reynolds number is increased to ~ 1 [Fig. 15.1b], the effective cross section gets reduced to roughly the cylinder's geometrical width d, and correspondingly the drag coefficient decreases to $C_D \sim 1$. At this Reynolds number, $\mathrm{Re}_d \sim 1$, the velocity field begins to appear asymmetric from front to back.

With a further increase in Re_d, a laminar boundary layer of thickness $\delta \sim d/\sqrt{\mathrm{Re}_d}$ starts to form. The viscous force per unit length due to this boundary layer is $F \sim \rho V^2 d/\sqrt{\mathrm{Re}_d}$ [Eqs. (14.46)–(14.48) divided by w, with $\ell \sim d$ and $v_o = V$]. It might therefore be thought that the drag would continue to decrease as $C_D \sim 1/\sqrt{\mathrm{Re}_d}$, when Re_d increases substantially above unity making the boundary layer thin and making the external flow start to resemble potential flow. However, this does *not* happen. Instead, at $\mathrm{Re}_d \sim 5$, the flow begins to separate from the back side of the cylinder and is there replaced by two retrograde eddies (Fig. 15.1c). As described in Sec. 14.4.3, this separation occurs because an adverse pressure gradient $(\mathbf{v}\cdot\boldsymbol{\nabla})P > 0$ develops outside the boundary layer, near the cylinder's downstream face, and causes the separated boundary layer to be replaced by these two

counter-rotating eddies. The pressure in these eddies, and thus also on the cylinder's back face, is of order the flow's incoming pressure P_0 and is significantly less than the stagnation pressure $P_{\rm stag} = P_0 + \frac{1}{2}\rho V^2$ at the cylinder's front face, so the drag coefficient stabilizes at $C_D \sim 1$.

As the Reynolds number increases above $\mathrm{Re}_d \sim 5$, the size of the two eddies increases until, at $\mathrm{Re}_d \sim 100$, the eddies are shed dynamically, and the flow becomes non-stationary. The eddies tend to be shed alternately in time, first one and then the other, producing a beautiful pattern of alternating vortices downstream known as a *Karman vortex street* (Fig. 15.1d).

When $\mathrm{Re}_d \sim 1000$, the downstream vortices are no longer visible and the wake behind the cylinder contains a velocity field irregular on all scales (Fig. 15.1e). This downstream flow has become turbulent. Finally, at $\mathrm{Re}_d \sim 3 \times 10^5$, the boundary layer, which has been laminar up to this point, itself becomes turbulent (Fig. 15.1f), reducing noticeably the drag coefficient (Fig. 15.2). We shall explore the cause of this reduction below. [The physically relevant Reynolds number for onset of turbulence in the boundary layer is that computed not from the cylinder diameter d, $\mathrm{Re}_d = Vd/\nu$, but rather from the boundary layer thickness $\delta \sim d/\mathrm{Re}_d^{1/2}$:

$$\boxed{\mathrm{Re}_\delta = \frac{V\delta}{\nu} \sim \frac{Vd\mathrm{Re}_d^{-1/2}}{\nu} = \sqrt{\mathrm{Re}_d}} \,. \tag{15.7}$$

The onset of boundary-layer turbulence is at $\mathrm{Re}_\delta \sim \sqrt{3 \times 10^5} \sim 500$, about the same as the $\mathrm{Re}_d \sim 1000$ for onset of turbulence in the wake.]

An important feature of this changing flow pattern is the fact that at $\mathrm{Re}_d \ll 1000$ (Figs. 15.1a–d), before any turbulence sets in, the flow (whether steady or dynamical) is translation symmetric; i.e., it is independent of distance z down the cylinder; i.e., it is two-dimensional. This is true even of the Karman vortex street. By contrast, the turbulent velocity field at $\mathrm{Re}_d \gtrsim 1000$ is fully three-dimensional. At these large Reynolds numbers, small, non-translation-symmetric perturbations of the translation-symmetric flow grow into vigorous, three-dimensional turbulence. This is a manifestation of the fact (which we shall explore below) that two-dimensional flows cannot exhibit true turbulence. True turbulence requires chaotic motions in all three dimensions.

The most important feature of this family of flows, a feature that is characteristic of most such families, is that there is a critical Reynolds number for the onset of turbulence. That critical number can range from ~ 30 to $\sim 10^5$, depending on the geometry of the flow and on precisely what length and speed are used to define the Reynolds number.

****

EXERCISES

Exercise 15.1 ****Example: The 2-Dimensional Laminar Wake Behind a Cylinder*
In Ex. 15.5 below, we shall explore the structure of the wake behind the cylinder when the Reynolds number is high enough that the flow is turbulent. For comparison, we here compute the wake's structure at lower Reynolds numbers, when the wake is laminar. This

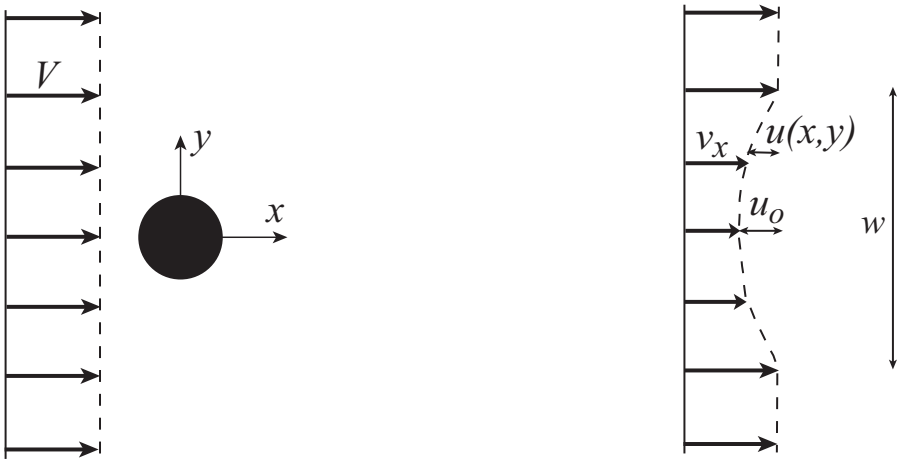

Fig. 15.3: The two-dimensional laminar wake behind an infinite cylinder. ambient fluid.

computation is instructive: it illustrates using order of magnitude estimates first, followed by detailed calculations, it illustrates the power of momentum conservation, and it is our first encounter with the velocity field in a wake.

(a) Begin with an order of magnitude estimate. Characterize the wake by its width $w(x)$ at distance x downstream from the cylinder, and by the reduction in the flow velocity (the "velocity deficit"), $u_o(x) \equiv V - v_x(x)$, at the center of the wake; see Fig. 15.3. From diffusion of vorticity show that $w \simeq 2\sqrt{\nu x/V}$.

(b) Explain why momentum conservation says the force per unit length on the cylinder, $F_D = C_D \frac{1}{2}\rho V^2 d$ [Eq. (15.6)], is equal to the transverse integral $\int T_{xx} dy$ of the fluid's kinetic stress $T_{xx} = \rho v_x v_x$ before the fluid reaches the sphere, minus that integral at distance x after the sphere. Use this to show that the fractional velocity deficit at the center of the wake is $u_o/V \simeq C_D d/w \simeq C_d\sqrt{d\,\mathrm{Re}_d/16x}$.

(c) For a more accurate description of the flow, solve the Navier Stokes equation to obtain the profile of the velocity deficit, $u(x,y) \equiv V - v_x(x,y)$. [Hint: the Navier Stokes should reduce to the one dimensional diffusion equation, which we have met several times previously in this book.] Your answer should be

$$u = u_o e^{-(2y/w)^2}\ , \quad \text{where } w = 4\left(\frac{\nu x}{V}\right)^{1/2} \quad \text{and } \frac{u_o}{V} = C_D\left(\frac{d\,\mathrm{Re}_d}{16\pi x}\right)^{1/2} \tag{15.8}$$

are more accurate values of the wake's width and its central velocity deficit.

Exercise 15.2 *Problem: The 3-dimensional Laminar Wake behind a Sphere*
Repeat Ex. 15.1 for the 3-dimensional laminar wake behind a sphere.

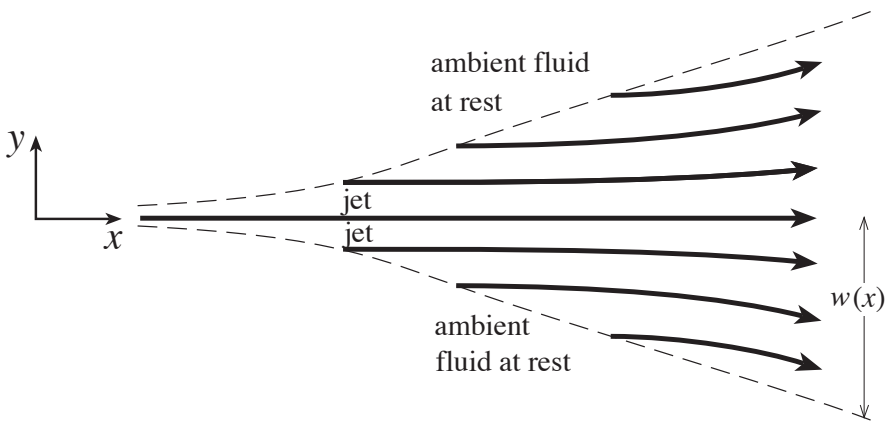

Fig. 15.4: Two-dimensional laminar jet. As the jet widens, it entrains ambient fluid.

Exercise 15.3 *Example: Structure of a 2-Dimensional Laminar Jet, and Entrainment*
Consider a narrow, two-dimensional, incompressible (i.e. subsonic) jet emerging from a two-dimensional nozzle into ambient fluid of the same composition and pressure, at rest. (By two-dimensional we mean that the nozzle and jet are translation symmetric in the third dimension.) Let the Reynolds number be low enough for the flow to be laminar; we shall study the turbulent regime in Ex. 15.6 below. We want to understand how rapidly this laminar jet spreads.

(a) Show that the pressure forces far downstream from the nozzle are likely to be much smaller than the viscous forces and can therefore be ignored.

(b) Let the jet's thrust per unit length (i.e. the momentum per unit time per unit length flowing through the nozzle) be $\mathcal{F}$. Introduce cartesian coordinates x, y, with x parallel to and y perpendicular to the jet (cf. Fig. 15.4). As in Ex. 15.1, use vorticity diffusion (or the Navier Stokes equation) and momentum conservation to estimate the speed v_x of the jet and its width w as functions of distance x downstream.

(c) Use these scalings to modify the self-similarity analysis of the Navier Stokes equation, that we used for the laminar boundary layer in Sec. 14.4, and thereby obtain the following approximate solution for the jet's velocity profile:

$$v_x = \left(\frac{3\mathcal{F}^2}{32\rho^2\nu x}\right)^{1/3} \mathrm{sech}^2\left(\left[\frac{\mathcal{F}}{48\rho\nu^2x^2}\right]^{1/3} y\right) . \tag{15.9}$$

(d) Equation (15.9) shows that the jet width w increases downstream as $x^{2/3}$. As the jet widens, it scoops up (entrains) ambient fluid as depicted in Fig. 15.4. This entrainment actually involves pulling fluid inward in a manner described by the y component of velocity, v_y. Solve the incompressiblity equation $\boldsymbol{\nabla}\cdot\mathbf{v} = 0$ to obtain the following

expression for v_y:

$$v_y = -\frac{1}{3x}\left(\frac{3\mathcal{F}^2}{32\rho^2\nu x}\right)^{1/3} \times\left\{\left(\frac{48\rho\nu^2x^2}{\mathcal{F}}\right)^{1/3}\tanh\left(\left[\frac{\mathcal{F}}{48\rho\nu^2x^2}\right]^{1/3}y\right) - 2y\,\mathrm{sech}^2\left(\left[\frac{\mathcal{F}}{48\rho\nu^2x^2}\right]^{1/3}y\right)\right\} \simeq -\left(\frac{1}{6}\frac{\mathcal{F}\nu}{\rho x^2}\right)^{1/3}\mathrm{sign}(y) \quad \text{at } |y| \gg w(x) = \left(\frac{48\rho\nu^2x^2}{\mathcal{F}}\right)^{1/3} . \tag{15.10}$$

Thus, ambient fluid is pulled inward from both sides to satisfy the jet's entrainment appetite.

****

15.3 Empirical Description of Turbulence

Empirical studies of turbulent flows have revealed a number of universal properties that are best comprehended through movies (Box 15.2). Here we shall simply list the most important of them, and comment on them briefly. We shall revisit most of them in more detail in the remainder of the chapter. Throughout, we shall restrict ourselves to turbulence with velocities that are very subsonic and thus incompressible.

Turbulence is characterized by:

- *Disorder, irreproducible in detail but with rich, non-random structure.* This disorder is intrinsic to the flow. It appears to arise from a variety of instabilities. No forcing by external agents is required to produce it. If we try to resolve the flow into modes, however, we find that the phases of the modes are *not* fully random, either spatially or temporally. There are strong correlations. Correspondingly, if we look at a snapshot of a turbulent flow, we frequently observe large, well-defined coherent structures like eddies and jets, which suggests that the flow is more organized than a purely random superposition of modes, just as the light reflected from the surface of a painting differs from that emitted by a black body. if we monitor the time variation of some fluid variable, such as one component of the velocity at a given point in the flow, we observe *intermittency* – the irregular starting and ceasing of strong turbulence. Again, this is such a marked effect that there is more than a random-mode superposition at work, reminiscent of the distinction between noise and music (at least some music). [A major consequence that we shall have to face is this: Strong turbulence is *not* well treated by perturbation theory. Alternative, semi-quantitative techniques of analysis must be devised.]

- *A wide range of interacting scales.* When the fluid velocity and pressure are Fourier analyzed, one finds them varying strongly over many decades of wave number and

frequency. We can think of these variations as due to *eddies* with a huge range of sizes. These eddies interact strongly. Typically, large eddies appear to feed their energy to smaller eddies, which in turn feed energy to still smaller eddies, and so forth. Occasionally, amazingly, the flow of energy appears to reverse: small-scale turbulent structures give rise to large-scale structures, resulting in intermittency. A region of the flow that appears to have calmed down may suddenly and unexpectedly become excited again.

- *Vorticity, irregularly distributed in three dimensions.* This vorticity varies in magnitude and direction over the same wide range of scales as the fluid velocity. It appears to play a central role in coupling large scales to small; see the next subsection.

- *Large dissipation*: Typically, turbulent energy is fed from large scales to small in just one turnover time of a large eddy. This is extremely fast. The energy cascades downward to smaller and smaller scales until it reaches eddies so small that their shear, coupled to molecular viscosity, converts the turbulent energy into heat.

- *Efficient mixing and transport* of most everything that can be transported: momentum, heat, salt, chemicals, ...

15.3.1 The Role of Vorticity in Turbulence

Turbulent flows contain tangled vorticity. As we discussed in Sec. 14.2.2, when viscosity is unimportant, vortex lines are frozen into the fluid and can be stretched by the action of neighboring vortex lines. As a bundle of vortex lines is stretched and twisted (Fig. 15.5), the incompressibility of the fluid causes the bundle's cross section to decrease and correspondingly causes the magnitude of its vorticity to increase, and the lengthscale on which the vorticity changes to decrease (cf. Sec. 14.2). The continuous lengthening and twisting of the fluid therefore creates vorticity on progressively smaller length scales.

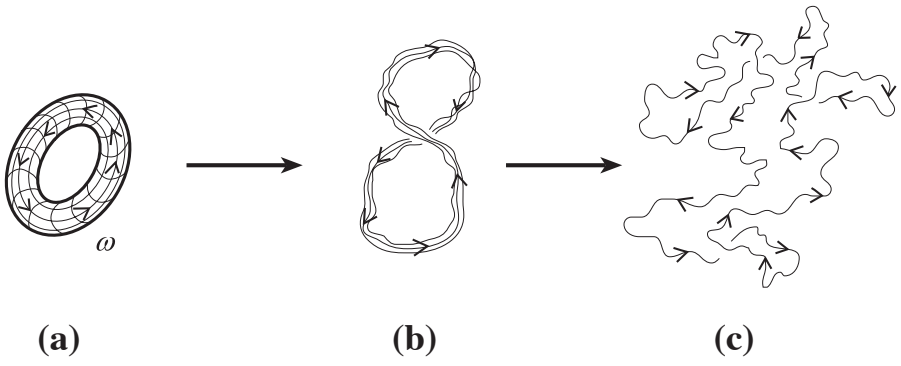

Fig. 15.5: Schematic illustration of the propagation of turbulence by the stretching of vortex lines. The tube of vortex lines in (a) gets stretched and thereby is forced into a reduced cross section by the turbulent evolution from (a) to (b) to (c). The reduced cross section means an enhanced vorticity on smaller scales.

Note that, when the flow is two-dimensional (i.e. translation symmetric), there is no stretching of the vortex lines and thus no inexorable driving of the turbulent energy to smaller and smaller length scales. This is one reason why true turbulence does not occur in two dimensions, only in three.

On the other hand, something akin to turbulence, but with much less richness and small scale structure, *does* occur in two dimensions, as one sees, e.g., in two-dimensional simulations of the Kelvin-Helmholtz instability, Box 15.3. However, in the real world, once the Kelvin-Helmholtz instability gets well developed, three-dimensional instabilities grow strong, vortex-line stretching grows strong, and the flow develops full three-dimensional turbulence. The same happens in other ostensibly two-dimensional flow, e.g. the "two-dimensional" wake behind a long circular cylinder and "two-dimensional" jets and boundary layers(Secs. 15.4.3 and 15.5).

Box 15.3
Consequences of the Kelvin-Helmholtz Instability

The Kelvin-Helmholtz instability arises when two fluids, with nearly the same density, are in uniform motion past each other (Sec. 14.6). Their interface (a vortex sheet) develops corrugations that grow (Figs. 14.17 and 14.18). That growth bends the corrugations more and more sharply. Along the corrugated interface the fluids on the two sides are still sliding past each other, so the instability arises again, on this smaller scale — and again and again: somewhat like the cascade of turbulent energy from large scales to small.

In the real world, three-dimensional instabilities also arise and the flow becomes fully turbulent. However, much insight is gained into the difference between two-dimensional and three-dimensional flow by artificially constraining the Kelvin-Helmholtz flow to remain two-dimensional. This is easily done in numerical simulations. Movies of such simulations abound on the web, e.g. in 2012 on the Wikipedia web page for the Kelvin-Helmholtz instability. The following picture is a still from that movie:

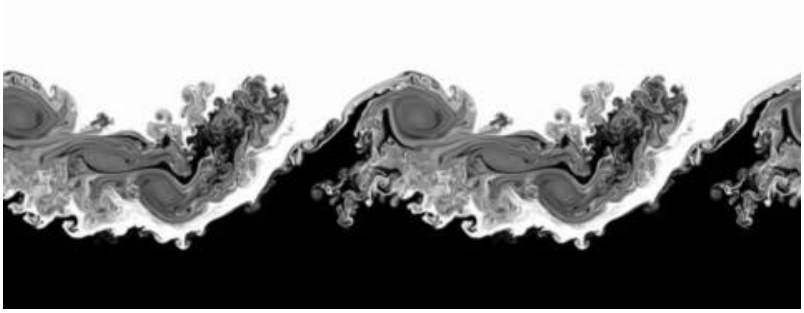

Although the structures in this simulation are rich, they are much less rich than those that appear in full, three-dimensional turbulence — perhaps largely due to the absence of stretching and twisting of vortex lines, when the flow is confined to two dimensions. [Note: Not surprisingly, the structures in this simulation resemble some in Jupiter's atmosphere, which also arise from a Kelvin-Helmholtz instability.]

15.4 Semi-Quantitative Analysis of Turbulence

In this section we shall develop a semi-quantititative mathematical analysis of turbulence and explore a few applications. This analysis is fairly good for so-called *weak turbulence*. However for the much more common *strong turbulence*, it is at best semi-quantitative — but nonetheless is widely used for lack of anything simple that is much better.

15.4.1 Weak Turbulence Formalism

The meaning of weak turbulence can be explained in terms of interacting eddies (a concept we shall exploit in Sec. 15.4.4 when studying the flow of turbulent energy from large scales to small). One can regard turbulence as weak if the timescale τ_* for a big eddy to feed most of its energy to smaller eddies is long compared to the big eddy's turnover time τ, i.e., its "rotation period". The weak-turbulence formalism (model) that we shall sketch in this subsection can be thought of as an expansion in τ/τ_*.

Unfortunately, for most turbulence seen in fluids, the large eddies' energy loss time is of order its turnover time, $\tau/\tau_* \sim 1$, which means the eddy loses its identity in roughly one turnover time, and the turbulence is strong. In this case, the weak-turbulence formalism that we shall sketch here is only semiquantitatively accurate.

Our formalism for weak turbulence (with gravity negligible and the flow very subsonic so it can be regarded as incompressible) is based on the standard incompressibility equation and the time-dependent Navier-Stokes equation, which we write in the following forms:

$$\boldsymbol{\nabla}\cdot\mathbf{v} = 0\,, \tag{15.11a}$$

$$\rho\frac{\partial\mathbf{v}}{\partial t} + \boldsymbol{\nabla}\cdot(\rho\mathbf{v}\otimes\mathbf{v}) = -\boldsymbol{\nabla}P + \rho\nu\nabla^2\mathbf{v}\,. \tag{15.11b}$$

[Eq. (15.11b) is equivalent to (15.2b) with $\partial\mathbf{v}/\partial t$ added because of the time dependence, and with the inertial force term rewritten via $\boldsymbol{\nabla}\cdot(\rho\mathbf{v}\otimes\mathbf{v}) = \rho(\mathbf{v}\cdot\boldsymbol{\nabla})\mathbf{v}$, or equivalently in index notation, $(\rho v_i v_j)_{;i} = \rho_{,i}v_i v_j + \rho(v_{i;i}v_j + v_i v_{j;i}) = \rho v_i v_{j;i}$.] Equations (15.11) are four scalar equations for four unknowns, $P(\mathbf{x},t)$ and the three components of $\mathbf{v}(\mathbf{x},t)$; ρ and ν can be regarded as constants.

To obtain the weak-turbulence versions of these equations, we split the velocity field $\mathbf{v}(\mathbf{x},t)$ and pressure $P(\mathbf{x},t)$ into steady parts $\bar{\mathbf{v}}$, $\bar{P}$, plus fluctuating parts, $\delta\mathbf{v}$, δP:

$$\boxed{\mathbf{v} = \bar{\mathbf{v}} + \delta\mathbf{v}\,,\quad P = \bar{P} + \delta P}\,. \tag{15.12}$$

We can think of (or, in fact, define) $\bar{\mathbf{v}}$ and $\bar{P}$ as the time averages of $\mathbf{v}$ and P, and define $\delta\mathbf{v}$ and δP as the difference between the exact quantities and the time-averaged quantities.

The time-averaged variables $\bar{\mathbf{v}}$ and $\bar{P}$ are governed by the time averages of the incompressibility and Navier-Stokes equations (15.11). Because the incompressibility equation is linear, its time average

$$\boxed{\boldsymbol{\nabla}\cdot\bar{\mathbf{v}} = 0} \tag{15.13a}$$

entails no coupling of the steady variables to the fluctuating variables. By contrast, the nonlinear inertial term $\boldsymbol{\nabla}\cdot(\rho\mathbf{v}\otimes\mathbf{v})$ in the Navier-Stokes equation gives rise to such a coupling

in the (time-independent) time-averaged equation:

$$\boxed{\rho(\bar{\mathbf{v}}\cdot\boldsymbol{\nabla})\bar{\mathbf{v}} = -\boldsymbol{\nabla}\bar{P} + \nu\rho\nabla^2\bar{\mathbf{v}} - \boldsymbol{\nabla}\cdot\mathbf{T}_R}\,. \tag{15.13b}$$

Here

$$\boxed{\mathbf{T}_R \equiv \rho\overline{\delta\mathbf{v}\otimes\delta\mathbf{v}}} \tag{15.13c}$$

is known as the *Reynolds stress tensor*. It serves as a "driving term" in the time-averaged Navier-Stokes equation (15.13b) — a term by which the fluctuating part of the flow acts back on, and influences the time-averaged flow.

This Reynolds stress $\mathbf{T}_R$ can be regarded as an additional part of the total stress tensor, analogous to the gas pressure computed in kinetic theory,[3] $P = \frac{1}{3}\rho\overline{v^2}$, where v is the molecular speed. $\mathbf{T}_R$ will be dominated by the largest eddies present, and it can be anisotropic, especially when the largest-scale turbulent velocity fluctuations are distorted by interaction with an averaged shear flow, i.e when $\bar{\sigma}_{ij} = \frac{1}{2}(\bar{v}_{i;j} + \bar{v}_{j;i})$ is large.

If the turbulence is both stationary and homogeneous (a case we shall specialize to below when studying the "Kolmogorov spectrum"), then the Reynolds stress tensor can be written in the form $\mathbf{T}_R = P_R\mathbf{g}$, where P_R is the Reynolds pressure, which is independent of position, and $\mathbf{g}$ is the metric, so $g_{ij} = \delta_{ij}$. In this case, the turbulence will exert no force density on the mean flow; i.e., $\boldsymbol{\nabla}\cdot\mathbf{T}_R = \boldsymbol{\nabla}P_R$ will vanish in the time-averaged Navier-Stokes equation (15.13b). By contrast, near the edge of a turbulent region (e.g., near the edge of a turbulent wake or jet or boundary layer), the turbulence will be inhomogeneous, and thereby (as we shall see in the next subsection) will exert an important influence on the time-independent, averaged flow.

Notice that the Reynolds stress tensor is the tensorial *correlation function* (also called "autocorrelation function") of the velocity fluctuation field at zero time delay (multiplied by density ρ); cf. Secs. 6.4.1 and 6.5.1. Notice also that it involves the temporal *cross-correlation function* of components of the velocity fluctuation, e.g. $\overline{\delta v_x(\mathbf{x},t)\delta v_y(\mathbf{x},t)}$ (Sec. 6.5.1). It is possible to extend this weak-turbulence formalism so it probes the statistical properties of turbulence more deeply, with the aid of correlation functions with finite time delays, and correlation functions of velocity components (or other relevant physical quantities) at two different points in space simultaneously. (It is relatively straightforward experimentally to measure these correlation functions.) As we discuss in greater detail below (and as we also saw for one- and two-dimensional random processes in Secs. 6.4.4 and 6.5.2, and for multidimensional, complex random processes in Ex. 9.7), the Fourier transforms of these correlation functions give the spatial and temporal spectral densities of the fluctuating quantities.

Just as the structure of the time-averaged flow is governed by the time-averaged incompressibility and Navier-Stokes equations (15.13) (with the fluctuating variables acting on the time-averaged flow through the Reynolds stress), so also the fluctuating part of the flow is governed by the fluctuating (difference between exact and time-averaged) incompressibility and Navier-Stokes equations. For details, see Ex. 15.4. This is an important exercise; it exhibits the weak-turbulence formalism in action, and underpins the application to spatial energy flow in a 2-dimensional, turbulent wake in Fig. 15.7 below.

[3]Deducible from Eq. (3.35c) or from Eqs. (3.37b) and (3.37c) with mean energy per particle $\bar{E} = \frac{1}{2}m\overline{v^2}$.

****

EXERCISES

Exercise 15.4 ****Example: Reynolds Stress, and Fluctuating Part of Navier-Stokes Equation in Weak Turbulence*

(a) Derive the time-averaged Navier-Stokes equation (15.13b) from the time-dependent form of the equation, (15.11b), and thereby infer the definition (15.13c) for the Reynolds stress. Equation (15.13b) shows how the Reynolds stress affects the evolution of the mean velocity. However, it does not tell us how the Reynolds stress evolves.

(b) Explain why an equation for the evolution of the Reynolds stress must involve averages of triple products of the velocity fluctuation. Similarly the time evolution of the averaged triple products will involve averaged quartic products, and so on (cf. the BBGYK hierarchy of equations in plasma physics, Sec. 21.6). How do you think you might "close" this sequence of equations, i.e. terminate it at some low order and get a fully determined system of equations? [Hint: the simplest way is via the turbulent viscosity of the next Section.]

(c) Show that the fluctuating part of the Navier-Stokes equation (the difference between the exact Navier-Stokes equation and its time average) takes the following form:

$$\boxed{\frac{\partial \delta\mathbf{v}}{\partial t} + (\bar{\mathbf{v}}\cdot\boldsymbol{\nabla})\delta\mathbf{v} + (\delta\mathbf{v}\cdot\boldsymbol{\nabla})\bar{\mathbf{v}} + [(\delta\mathbf{v}\cdot\boldsymbol{\nabla})\delta\mathbf{v} - \overline{(\delta\mathbf{v}\cdot\boldsymbol{\nabla})\delta\mathbf{v}}] = -\frac{1}{\rho}\boldsymbol{\nabla}\delta P + \nu\nabla^2(\delta\mathbf{v})}\,. \tag{15.14a}$$

This equation and the fluctuating part of the incompressibility equation

$$\boxed{\boldsymbol{\nabla}\cdot\delta\mathbf{v} = 0} \tag{15.14b}$$

govern the evolution of the fluctuating variables $\delta\mathbf{v}$ and δP. [The challenge, of course, is to devise ways to solve these equations despite the nonlinearities and the coupling to the mean flow that show up strongly in Eq. (15.14a).]

(d) By dotting $\delta\mathbf{v}$ into Eq. (15.14a) and then taking its time average, derive the following law for the spatial evolution of the turbulent energy density $\frac{1}{2}\rho\overline{\delta v^2}$:

$$\boxed{\bar{\mathbf{v}}\cdot\boldsymbol{\nabla}(\frac{1}{2}\rho\overline{\delta v^2}) + \boldsymbol{\nabla}\cdot\overline{\left(\frac{1}{2}\rho\delta v^2\delta\mathbf{v} + \delta P\delta\mathbf{v}\right)} = -T_R^{ij}\bar{v}_{i,j} + \nu\rho\overline{\delta\mathbf{v}\cdot(\nabla^2\delta\mathbf{v})}}\,. \tag{15.15}$$

Here $T_R^{ij} = \rho\overline{\delta v_i \delta v_j}$ is the Reynolds stress [Eq. (15.13c)]. Interpret each term in this equation. [The four interpretations will be discussed below, for a 2-dimensional turbulent wake, in connection with Fig. 15.7.]

(e) Now derive a similar law for the spatial evolution of the energy density of ordered motion $\frac{1}{2}\rho\bar{\mathbf{v}}^2$. Show that the energy lost by the ordered motion is compensated by the energy gained by the turbulent energy.

****

15.4.2 Turbulent Viscosity

Additional tools that are often introduced in the theory of weak turbulence come from taking the analogy with the kinetic theory of gases one stage further and defining *turbulent transport coefficients* (most importantly a turbulent viscosity that governs the turbulent transport of momentum). These turbulent transport coefficients are derived by simple analogy with the kinetic-theory transport coefficients (Sec. 3.7.) Momentum, heat, etc. are transported most efficiently by the largest turbulent eddies in the flow; therefore, in estimating the transport coefficients we replace the particle mean free path by the size ℓ of the largest eddies and the mean particle speed by the magnitude v_ℓ of the fluctuations of velocity in the largest eddies. The result, for momentum transport, is a model turbulent viscosity

$$\boxed{\nu_t \simeq \frac{1}{3} v_\ell \ell} \tag{15.16}$$

[cf. Eq. (13.72) for molecular viscosity, with $\nu = \eta/\rho$]. The Reynolds stress is then approximated as a turbulent shear stress of the standard form

$$\boxed{\mathbf{T}_R \simeq -2\rho\nu_t \bar{\boldsymbol{\sigma}}} \,. \tag{15.17}$$

Here $\bar{\boldsymbol{\sigma}}$ is the rate of shear tensor (13.63b) evaluated using the mean velocity field $\bar{\mathbf{v}}$. Note that the turbulent kinematic viscosity defined in this manner, ν_t, is a property of the turbulent flow and not an intrinsic property of the fluid; it differs from molecular viscosity in this important respect.

We have previously encountered turbulent viscosity in our study of the physical origin of the Sargasso-Sea gyre in the north Atlantic Ocean and the gyre's role in generating the Gulf Stream (Ex. 14.12). The gyre is produced by water flowing in a wind-driven Ekman boundary layer at the ocean's surface. From the measured thickness of that boundary layer, $\delta_E \sim 30$ meters, we deduced that the boundary layer's viscosity is orders of magnitude larger than water's molecular viscosity; it is the turbulent viscosity of Eq. (15.16).

By considerations similar to those above for turbulent viscosity, one can define and estimate a turbulent thermal conductivity for the spatial transport of time-averaged heat (cf. Sec. 3.7.2) and a turbulent diffusion coefficient for the spatial transport of one component of a time-averaged fluid through another, for example an odor crossing a room (cf. Ex. 3.19).

The turbulent viscosity ν_t and the other turbulent transport coefficients can be far far larger than their kinetic-theory values. One example is the Ekman boundary layer that drives water to pile up in the north-Atlantic Sargasso Sea (discussed above). Another is air in a room subjected to typical uneven heating and cooling. The air may typically circulate

with an average largest eddy velocity of $v_\ell \sim 1$ cm s^{-1} and an associated eddy size of $\ell \sim 3$ m. (This can be estimated by observing the motion of illuminated dust particles.) The kinematic turbulent viscosity ν_t — and also the turbulent diffusion coefficient D_t (Ex. 3.19) — associated with these motions are $\nu_t \sim D_t \sim 10^{-2}$ m^2 s^{-1}, some three orders of magnitude larger than the molecular values.

15.4.3 Turbulent Wakes and Jets; Entrainment, and the Coanda Effect

As instructive applications of turbulent viscosity and related issues, we shall now explore in an order-of-magnitude way the structures of turbulent wakes and jets. The more complicated extension to a turbulent boundary layer will be explored in Sec. 15.5 below. In this section we focus on the 2-dimensional wake behind a cylinder. In Exs. 15.5, 15.6 and 15.7, we study the 3-dimensional wake behind a sphere, and 2- and 3-dimensional jets.

Order-of-magnitude Computation of Width and Velocity Deficit for a 2-Dimensional Turbulent Wake; Entrainment

For the wake behind a cylinder, depicted in Fig. 15.3 above, we begin by deducing the turbulent viscosity $\nu_t \sim \frac{1}{3} v_\ell \ell$. It is reasonable to expect, and observations confirm, that the largest eddies in a turbulent wake, at distance x past the cylinder, extend transversely across nearly the entire width $w(x)$ of the wake, so their size is $\ell \sim w(x)$. What is the largest eddies' circulation speed v_ℓ? Because these eddies' energies are fed into smaller eddies in (roughly) one eddy turnover time, these eddies must be continually regenerated by interaction between the wake and the uniform flow at its transverse boundaries. This means that the wake's circulation velocity v_ℓ cannot care about the velocity difference V between the incoming flow and the cylinder, way back upstream; the wake has long since lost memory of that. The only characteristic speed the wake knows about is the difference between its own mean downstream speed $\bar{v}_x$ and the speed V of the unform flow at its boundaries. It seems physically reasonable that the interaction between these two flows will drive the eddy to circulate with that difference speed, the *deficit* u_o depicted in Fig. 15.3, and observations show this to be true. Thus, $v_\ell \sim u_o$. This means that the turbulent viscosity is $\nu_t \sim \frac{1}{3} v_\ell \ell \sim \frac{1}{3} u_o(x) w(x)$.

Knowing the viscosity, we can compute our two unknowns, the wake's velocity deficit $u_o(x)$ and its width $w(x)$, from vorticity diffusion and momentum conservation, as we did for a laminar wake in Ex. 15.1a,b.

Consider, first, momentum conservation. Here, as in Ex. 15.1b, the drag force per unit length on the cylinder $F_D = C_D \frac{1}{2} \rho V^2 d$, must be equal to the difference between the momentum per unit length $\int \rho V^2 dy$ in the water impinging on the cylinder, and that $\int \rho v_x^2 dy$ at any chosen distance x behind the cylinder. That difference is easily seen, from Fig. 15.3, to be $\sim \rho V u_o w$. Equating this to F_D, we obtain the product $u_o w$ and thence $\nu_t \sim \frac{1}{3} u_o w \sim \frac{1}{6} C_D V d$.

Thus, remarkably, the turbulent viscosity is independent of distance x downstream from the cylinder. This means that the wake's vorticity (which is contained primarily in its large eddies) will diffuse transversely in just the manner we have encountered several times before

[Sec. 14.2.5, Eq. (14.37), Ex. 15.1a], causing its width to grow as $w \sim \sqrt{\nu_t x/V}$. Inserting $\nu_t \sim \frac{1}{6} C_D V d \sim \frac{1}{3} u_o w$ from above, we obtain

$$w \sim \left(\frac{C_D d}{6} x\right)^{1/2} , \quad u_o \sim V \left(\frac{3 C_D d}{2x}\right)^{1/2} \tag{15.18}$$

for the width and velocity deficit in the turbulent wake.

In this analysis, our appeal to vorticity diffusion obscures the physical mechanism by which the turbulent wake widens downstream. That mechanism is *entrainment*, i.e. capturing of fluid from outside the wake into the wake (a phenomenon we met for a laminar jet in Ex. 15.3d). The inertia of the largest eddies enables them to sweep outward into the surrounding flow with a transverse speed that is a sizable fraction of their turnover speed, say $\frac{1}{6} v_\ell$ (with the 1/6 to get agreement with the diffusion argument). This means that, moving with the flow at speed V, the eddy widens via entrainment at a rate $dw/dt = V dw/dx \sim \frac{1}{6} v_\ell \sim \frac{1}{6} u_o$. Inserting $u_o \sim \frac{1}{2} V C_d d/w$ from momentum conservation and solving the resulting differential equation, we obtain the same wake width $w \sim \sqrt{C_D d\, x/6}$ as we got from our diffusion argument.

Distribution of Vorticity in the Wake; Irregularity of the Wake's Edge

The wake's fluid can be cleanly distinguished from the exterior, ambient fluid by vorticity: Ambient flow velocity $\mathbf{v}(\mathbf{x}, t)$ is vorticity-free; the wake has nonzero vorticity. If we look at the actual flow velocity and refrain from averaging, the only way a fluid element in the wake can acquire vorticity is via molecular diffusion. Molecular diffusion is so slow, that the boundary between a region with vorticity and one without (the boundary between the wake fluid and the ambient fluid) is very sharp. Sharp, yes, but straight, no! The wake's eddies, little as well as big, drive the boundary into a very crooked shape (Fig. 15.6). Correspondingly, the order-of-magnitude wake width $w \sim \sqrt{C_D d\, x/6}$ that we have derived is only the width of a thoroughly averaged flow and not at all the actual, local width of the wake.

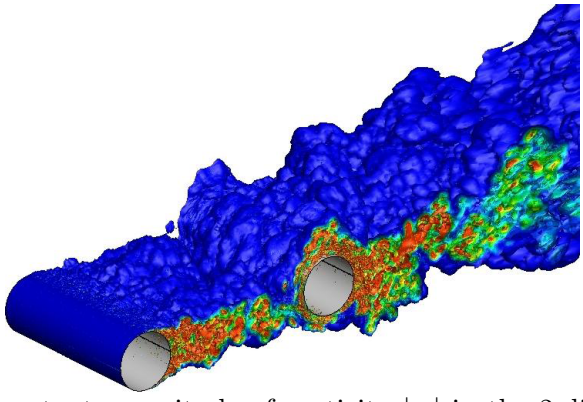

Fig. 15.6: Contours of constant magnitude of vorticity $|\boldsymbol{\omega}|$ in the 2-dimensional turbulent wake between and behind a pair of cylinders. The outer edge of the blue region is the edge of the wake. [From a numerical simulation by the research group of Sanjiva K. Lele at Stanford University, `http://flowgallery.stanford.edu/research.html`.]

Intermittency is one consequence of the wake's highly irregular edge. If one sits at a fixed location behind the cylinder, not too close to the wake's center, one will sometimes be outside the wake and sometimes inside it. This will show up in one's measurement of any flow variable, e.g., $v_y(t)$ or $\omega_x(t)$, or pressure P, at one's fixed location. When outside the wake, the measured quantities will be fairly constant; when inside, they will change rapidly and stochastically. The quiet epochs, with interspersed stochastic epochs are a form of intermittency.

Averaged Energy Flow in 2-Dimensional Turbulent Wake

The weak-turbulence formalism of Sec. 15.4.1 and Ex. 15.4 can be used to explore the generation and flow of turbulent energy in the wake behind a cylinder. The formalism, even when extended, is not good enough to make definitive predictions, but it *can* be used to deduce the energy flow from measurements of the mean (time averaged) flow velocity $\bar{\mathbf{v}}$, the turbulent velocity $\delta\mathbf{v}$ and the turbulent pressure δP. A classic example of this was carried out long ago by Albert Alan Townsend (1949) and is summarized in Fig. 15.7.

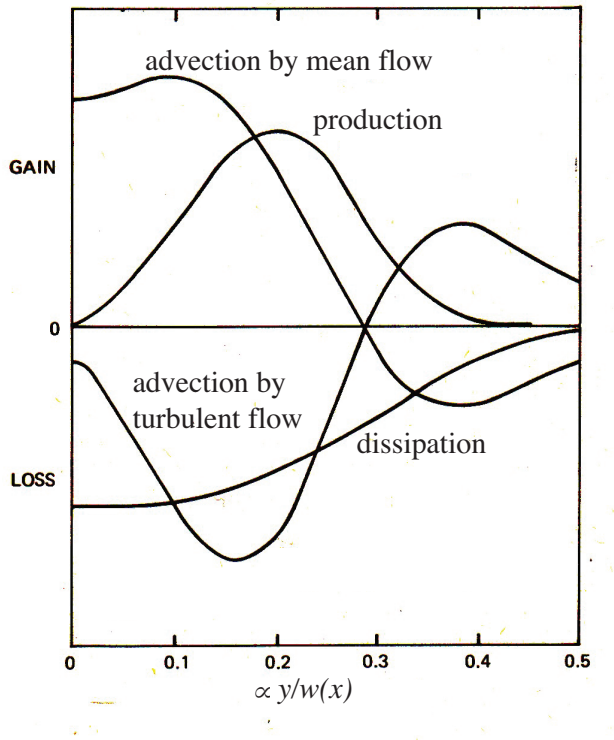

Fig. 15.7: The four terms in the rate of change of the time-averaged turbulent energy density [Eq. (15.15)] for the 2-dimensional turbulent wake behind a cylinder. Horizontal axis: distance y across the wake in units of the wake's mean width $w(x)$. Vertical axis: the numerical value of each term. For discussion of the four terms, see four bullets in the text. Energy conservation and stationarity of the averaged flow guarantee that the sum of the four terms vanishes at each y [Eq. (15.15)]. [Adapted from Fig. 22.10 of Tritton (1977), which is based on measurements and analysis by Townsend (1949).]

The time-averaged turbulent energy density changes due to four processes that are graphed in that figure as a function of distance y across the wake:

- ***Production:*** Energy in the organized bulk flow (mean flow) $\bar{\mathbf{v}}$ is converted into turbulent energy by interaction of the mean flow's shear with the turbulence's Reynold's stress, at a rate per unit volume $T^{ij}_{\rm R}\bar{v}_{i;j}$. This production vanishes at the wake's center ($y = 0$) because the shear of the mean flow vanishes there, and it vanishes at the edge of the wake because both the mean-flow shear and the Reynold's stress go to zero there.

- ***Advection by mean flow:*** Once produced, the turbulent energy gets advected across the wake by the mean flow. This causes an increase in turbulent energy density in the center of the wake and a decrease in the wake's outer parts, at a rate $\boldsymbol{\nabla}\cdot(\frac{1}{2}\rho\overline{\delta v^2}\bar{\mathbf{v}}) = (\bar{\mathbf{v}}\cdot\boldsymbol{\nabla})(\frac{1}{2}\rho\overline{\delta v^2})$.

- ***Advection by turbulent flow:*** Once produced, the turbulent energy also gets advected by the turbulent part of the flow, causing a decrease of turbulent energy density in the central regions of the wake and an increase in the outer regions, at a rate given by $\boldsymbol{\nabla}\cdot(\frac{1}{2}\rho\overline{\delta v^2\delta\mathbf{v}} + \overline{\delta P\delta\mathbf{v}})$.

- ***Dissipation:*** The turbulent energy gets converted to heat by molecular viscosity at a rate per unit volume given by $-\nu\rho\overline{\delta\mathbf{v}\cdot(\nabla^2\delta\mathbf{v})}$. This dissipation is largest at the wake's center and falls off gradually toward the wake's averaged edge.

Energy conservation, plus stationarity of the averaged flow, guarantees that the sum of these four terms vanishes at all locations in the wake (all y of Fig. 15.7). This is the physical content of Eq. (15.15) and is confirmed in Fig. 15.7 by the experimental data.

Entrainment and Coanda Effect

Notice how much wider the (averaged) turbulent wake is than the corresponding laminar wake of Ex. 15.1. The ratio of their widths [Eqs. (15.18) and (15.8)] is $w_t/w_l \sim \sqrt{C_D V d/\nu}$. For $C_D \sim 1$ in the turbulent wake, $V \sim 1$ m s^{-1}, $d \sim 1$ m, and water's kinematic viscosity $\nu \sim 10^{-6}$ m^2 s^{-1}, the ratio is $w_t/w_l \sim 10^3$, independent of distance x downstream. In this sense, entrainment in the turbulent wake is a thousand times stronger than entrainment in the laminar wake. Turbulent wakes and jets have voracious appetites for ambient fluid!

Entrainment is central to the *Coanda Effect*, depicted in Fig. 15.8: Consider a turbulent flow, e.g. the jet of Fig. 15.8, that is widening by entrainment of surrounding fluid. The jet normally widens downstream by pulling surrounding fluid into itself, and the inflow toward the jet extends far beyond the jet's boundaries (see, e.g., Ex. 15.3d). However, when there is a solid wall nearby, so there is no place for inflowing ambient fluid to come from, the jet's entrainment causes a drop in the pressure of the ambient fluid near the wall, and the resulting pressure gradient pushes the jet toward the wall as depicted in Fig. 15.8.

Similarly, if a turbulent flow is already close to a wall, and the wall begins to curve away from the flow, the flow develops a pressure gradient that tries to keep the turbulent region attached to the wall. In other words, *turbulent flows are attracted to solid surfaces and try to stick to them.* This is the *Coanda effect*.

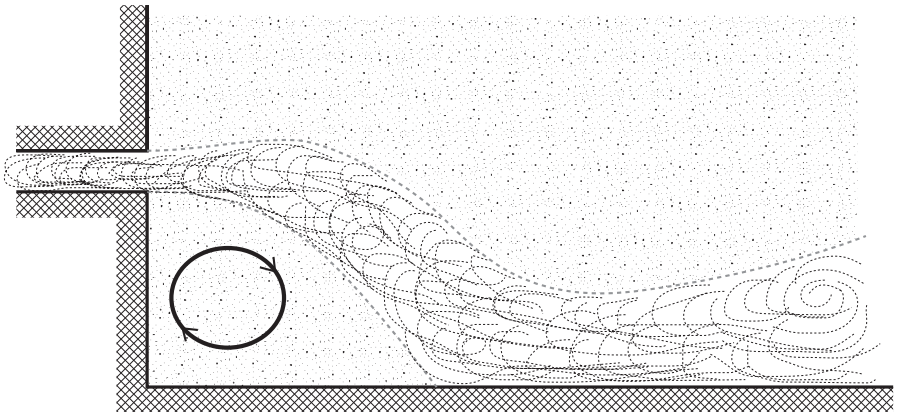

Fig. 15.8: The Coanda effect. A turbulent jet emerging from an orfice in the left wall is attracted by the solid bottom wall.

The Coanda effect also occur for laminar flows, but because entrainment is typically orders of magnitude weaker in laminar flows than turbulent, the Coanda effect is also orders of magnitude weaker.

The Coanda effect is important in aeronautics; for example, it is exploited to prevent the separation of the boundary layer from the upper surface of a wing, thereby improving the wing's lift and reducing its drag, as we shall discuss in Sec. 15.5.2 (Fig. 15.11).

****

EXERCISES

Exercise 15.5 *Problem: Turbulent Wake Behind a Sphere*
Compute the width $w(x)$ and velocity deficit $u_o(x)$ for the 3-dimensional turbulent wake behind a sphere.

Exercise 15.6 *Problem: Turbulent Jets in 2 and 3 Dimensions*
Consider a two-dimensional, turbulent jet emerging into an ambient fluid at rest, and contrast it to the laminar jet analyzed in Ex. 15.3.

(a) Find how the mean jet velocity and the jet width scale with distance downstream from the nozzle.

(b) Repeat the exercise for a three-dimensional jet.

Exercise 15.7 *Problem: Entrainment and Coanda Effect in a 3-Dimensional Jet*

(a) Evaluate the scaling of the rate of mass flow (discharge) $\dot{M}(x)$ along the three-dimensional, turbulent jet of the previous exercise. Show that $\dot{M}$ increases with distance from the nozzle so that mass must be entrained into the flow and become turbulent.

(b) Compare the entrainment rate for a turbulent jet with that for a laminar jet (Ex. 15.3). Do you expect the Coanda effect to be stronger for a turbulent or a laminar jet?

****

15.4.4 Kolmogorov Spectrum for Homogeneous and Isotropic Turbulence

When a fluid exhibits turbulence over a large volume that is well-removed from any solid bodies, then there will be no preferred directions and no substantial gradients in the statistically-averaged properties of the turbulent velocity field. This suggests that the turbulence will be stationary and isotropic. We shall now derive a semi-quantitative description of some of the statistical properties of such stationary, isotropic turbulence. Our derivation will be based on the following simple physical model:

We shall idealize the turbulent velocity field as made of a set of large eddies, each of which contains a set of smaller eddies and so on. We suppose that each eddy splits into eddies roughly half its size after a few turnover times. This can be described mathematically as nonlinear or triple velocity correlation terms [terms like the second one in Eq. (15.15)] producing, in the law of energy conservation, an energy transfer (a "cascade" of energy) from larger scale eddies to smaller scale eddies. Now, for large enough eddies, we can ignore the effects of molecular viscosity in the flow. However, for small enough eddies, viscous dissipation will convert the eddy bulk kinetic energy into heat. This simple model will enable us to derive a remarkably successful formula (the "Kolmogorov spectrum") for the distribution of turbulent energy over eddy size.

We must first introduce and define the turbulent energy per unit wave number and per unit mass, $u_k(k)$. For this purpose, we focus on a volume $\mathcal{V}$ much larger than the largest eddies. At some moment of time t, compute the spatial Fourier transform of the fluctuating part of the velocity field $\delta\mathbf{v}(\mathbf{x})$, confined to this volume [with $\delta\mathbf{v}(\mathbf{x})$ set to zero outside $\mathcal{V}$], and also write down the inverse Fourier transform:

$$\boxed{\delta\tilde{v}(\mathbf{k}) = \int_{\mathcal{V}} d^3x \delta\mathbf{v}(\mathbf{x}) e^{-i\mathbf{k}\cdot\mathbf{x}} \ , \quad \delta\mathbf{v} = \int \frac{d^3k}{(2\pi)^3} \delta\tilde{\mathbf{v}} e^{i\mathbf{k}\cdot\mathbf{x}} \quad \text{inside } \mathcal{V}} \ . \tag{15.19}$$

The total energy per unit mass u in the turbulence, averaged over the box $\mathcal{V}$, is then

$$u = \int \frac{d^3x}{\mathcal{V}} \frac{1}{2} \overline{|\delta\mathbf{v}|^2} = \int \frac{d^3k}{(2\pi)^3} \frac{\overline{|\delta\tilde{\mathbf{v}}|^2}}{2\mathcal{V}} \equiv \int_0^\infty dk \, u_k(k) \ , \tag{15.20}$$

where we have used Parseval's theorem in the second equality, we have used $d^3k = 4\pi k^2 dk$, and we have defined

$$u_k(k) \equiv \frac{\overline{|\delta\tilde{\mathbf{v}}|^2} k^2}{4\pi^2 \mathcal{V}} . \tag{15.21}$$

Here the bars denote a time average, k is the magnitude of the wave vector $k \equiv |\mathbf{k}|$ (i.e. it is the wave number or equivalently 2π divided by the wavelength), and $u_k(k)$ is called

the *spectral energy per unit mass* of the turbulent velocity field $\delta\mathbf{v}$. In the third equality in Eq. (15.20), we have assumed that the turbulence is isotropic so the integrand depends only on wave number k and not on the direction of $\mathbf{k}$. Correspondingly, we have defined $u_k(k)$ as the energy per unit wave number rather than an energy per unit volume of $\mathbf{k}$-space. This means that, $u_k(k)dk$ is the average kinetic energy per unit mass associated with modes that have k lying in the interval dk; we treat k as positive.

In Chap. 6 we introduced the concepts of a random process and its spectral density. The Cartesian components of the fluctuating velocity δv_x, δv_y, δv_z obviously are random processes that depend on vectorial location in space $\mathbf{x}$ rather than on time as in Chap. 6. It is straightforward to show that their *double sided* spectral densities are related to $u_k(k)$ by

$$\boxed{S_{v_x}(\mathbf{k}) = S_{v_y}(\mathbf{k}) = S_{\mathbf{v}_z}(k) = \frac{(2\pi)^2}{3k^2} \times u_k(k)} \,. \tag{15.22}$$

If we fold negative k_x into positive, and similarly for k_y and k_z so as to get the kind of single-sided spectral density that we used in Chap. 6, then these spectral densities get multiplied by $2^3 = 8$.

We shall now use our physical model of turbulence to derive an expression for $u_k(k)$. Denote by $k_{\rm min} = 2\pi/\ell$ the wave number of the largest eddies, and by $k_{\rm max}$ that of the smallest ones (those in which viscosity dissipates the cascading, turbulent energy). Our derivation will be valid, and the result will be valid, only when $k_{\rm max}/k_{\rm min} \gg 1$, i.e. only when there is a large sequence of eddies from the largest to half the largest to a quarter the largest ... down to the smallest.

As a tool in computing $u_k(k)$, we introduce the root-mean-square turbulent turnover speed of the eddies with wave number k, $v(k) \equiv v$; and ignoring factors of order unity, we treat the size of these eddies as k^{-1}. Then their turnover time is $\tau(k) \sim k^{-1}/v(k) = 1/[kv(k)]$. Our model presumes that in this same time τ (to within a factor of order unity), each eddy of size k^{-1} splits into eddies of half this size; i.e. the turbulent energy cascades from k to $2k$. In other words, our model presumes the turbulence is *strong*. Since the energy cascade is presumed stationary (i.e. no energy is accumulating at any wave number), the energy per unit mass that cascades in a unit time from k to $2k$ must be independent of k. Denote by q that k-independent, cascading energy per unit mass per unit time. Since the energy per unit mass in the eddies of size k^{-1} is v^2 (aside from a factor 2, which we neglect), and the cascade time is $\tau \sim 1/(kv)$, then $q \sim v^2/\tau \sim v^3 k$. This tells us that the rms turbulent velocity is

$$v(k) \sim (q/k)^{1/3}. \tag{15.23}$$

Our model lumps together all eddies with wave number within a range $\Delta k \sim k$ around k, and treats them all as having wave number k. The total energy per unit mass in these eddies is $u_k(k)\Delta k \sim k u_k(k)$ when expressed in terms of the sophisticated quantity $u_k(k)$, and it is $\sim v(k)^2$ when expressed in terms of our simple model. Thus, our model predicts that $u_k(k) \sim v(k)^2/k$, which by Eq. (15.23) implies

$$\boxed{u_k(k) \sim q^{2/3} k^{-5/3} \ \text{ for } k_{\rm min} \ll k \ll k_{\rm max}} \,; \tag{15.24}$$

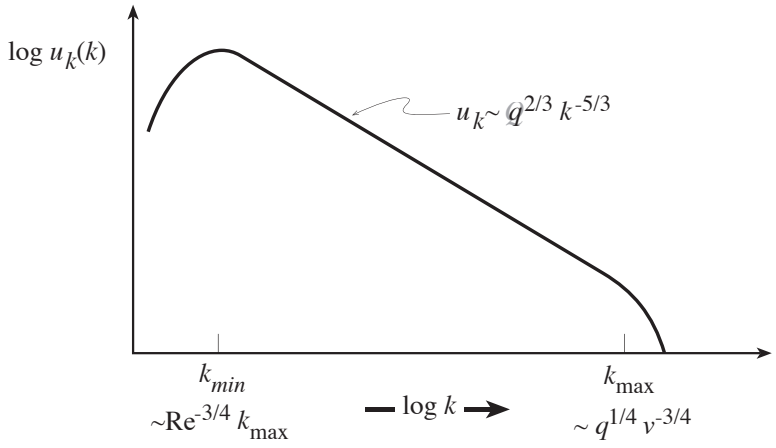

Fig. 15.9: The Kolmogorov spectral energy density for stationary, homogeneous turbulence.

see Fig. 15.9. This is the *Kolmogorov spectrum* for the spectral energy density of stationary, isotropic, incompressible turbulence. It is valid only in the range $k_{\rm min} \ll k \ll k_{\rm max}$ because only in this range are the turbulent eddies continuously receiving energy from larger lengthscales and passing it on to smaller scales. At the ends of the range, the spectrum will be modified in the manner illustrated qualitatively in Fig. 15.9.

The smallest lengthscales present, $k_{\rm max}^{-1}$, are determined by the fact that there molecular viscous forces become competitive with inertial forces in the Navier-Stokes equation, and thereby convert the cascading energy into heat. Since the ratio of inertial forces to viscous forces is the Reynolds number, the smallest eddies have a Reynolds number of order unity: $\mathrm{Re}_{k_{\rm max}} = v(k_{\rm max}) k_{\rm max}^{-1}/\nu \sim 1$. Inserting Eq. (15.23) for $v(k)$, we obtain

$$k_{\rm max} \sim q^{1/4} \nu^{-3/4}. \tag{15.25}$$

The largest eddies have sizes $\ell \sim k_{\rm min}^{-1}$ and turnover speeds $v_\ell = v(k_{\rm min}) \sim (q/k_{\rm min})^{1/3}$. By combining these relations with Eq. (15.25) we see that the ratio of the largest wave numbers present in the turbulence to the smallest is

$$\boxed{\frac{k_{\rm max}}{k_{\rm min}} \sim \left(\frac{v_\ell \ell}{\nu}\right)^{3/4} = \mathrm{Re}_\ell^{3/4}}. \tag{15.26}$$

Here Re_ℓ is the Reynolds number for the flow's largest eddies.

Let us now take stock of our results: If we know the scale ℓ of the largest eddies and their rms turnover speeds v_ℓ (and, of course, the viscosity of the fluid), then from these we can compute their Reynolds number Re_ℓ; from that, Eq. (15.26), and $k_{\rm min} \sim \ell^{-1}$, we can compute the flow's maximum and minimum wave numbers; and from $q \sim v_\ell^3/\ell$ and Eq. (15.24) we can compute the spectral energy density in the turbulence.

We can also compute the total time required for energy to cascade from the largest eddies to the smallest: Since $\tau(k) \sim 1/(kv) \sim 1/(q^{1/3} k^{2/3})$, each successive set of eddies feeds its energy downward in a time $2^{-2/3}$ shorter than the preceeding set. As a result, it takes roughly the same amount of time for energy to pass from the second largest eddies (size $\ell/2$)

to the very smallest (size $k_{\rm max}^{-1}$) as it takes for the second largest to extract the energy from the very largest. The total cascade occurs in a time of several ℓ/v_ℓ (during which time, of course, the mean flow has fed new energy into the largest eddies and they are sending it on downwards).

These results are accurate only to within factors of order unity – with one major exception: The $-5/3$ power law in the Kolmogorov spectrum is very accurate. That this ought to be so one can verify in two equivalent ways: (i) Repeat the above derivation inserting arbitrary factors of order unity at every step. These factors will influence the final multiplicative factor in the Kolmogorov spectrum, but will not influence the $-5/3$ power. (ii) Use dimensional analysis. Specifically: notice that the only dimensioned entitities that can influence the spectrum in the region $k_{\rm min} \ll k \ll k_{\rm max}$ are the energy cascade rate q and the wave number k. Then notice that the only quantity with the dimensions of $u_k(k)$ (energy per unit mass per unit wave number) that can be constructed from q and k is $q^{2/3}k^{-5/3}$. Thus, aside from a multiplicative factor of order unity, this must be the form of $u_k(k)$.

Let us now review and critique the assumptions that went into our derivation of the Kolmogorov spectrum. First, we assumed that the turbulence is stationary and homogeneous. Real turbulence is neither of these, since it exhibits *intermittency* (Sec. 15.3), and smaller eddies tend to occupy less volume overall than larger eddies and so cannot be uniformly distributed in space. Second, we assumed that the energy source is large-length-scale motion and that the energy transport is local in k-space from the large length scales to steadily smaller ones. In the language of a Fourier decomposition into normal modes, we assumed that nonlinear coupling between modes with wave number k causes modes with wave number of order $2k$ to grow, but does not significiantly enhance modes with wave number $100k$ or $0.01k$. Again this is not completely in accord with observations which reveal the development of *coherent structures*–large scale regions with correlated vorticity in the flow. These structures are evidence for a reversed flow of energy in k-space from small scales to large scales, and they play a major role in another feature of real turbulence, *entrainment* – the spreading of an organised motion, e.g. a jet, into the surrounding fluid (Sec. 15.4.3 above).

Despite these qualifications, the Kolmogorov law is surprisingly useful. It has been verified in many laboratory flows, and it describes many naturally occuring instances of turbulence. For example, the twinkling of starlight is caused by refractive index fluctuations in the earth's atmosphere, whose power spectrum we can determine optically. The underlying turbulence spectrum turns out to be of Kolmogorov form.

****

EXERCISES

Exercise 15.8 *Example: Excitation of Earth's Normal Modes by Atmospheric Turbulence*[4]
The Earth has normal modes of oscillation, many of which are in the milliHertz frequency range. Large earthquakes occasionally excite these modes strongly, but the quakes are usually

[4]Problem devised by David Stevenson; based in part on Tanimoto and Um (1999) who, however, use the pressure spectrum deduced in part (i) rather than the more nearly correct spectrum of part (ii). The difference in spectra does not much affect their conclusions

widely spaced in time compared to the ringdown time of a particular mode (typically a few days). There is evidence of a background level of continuous excitation of these modes, with an rms ground acceleration per mode $\sim 10^{-10}$ cm/s^2 at seismically "quiet" times. Stochastic forcing by the pressure fluctuations associated with atmospheric turbulence is suspected. This exercise deals with some aspects of this hypothesis.

(a) Estimate the rms pressure fluctuations $P(f)$ at frequency f, in a bandwidth equal to frequency $\Delta f = f$, produced on the earth's surface by atmospheric turbulence, assuming a Kolmogorov spectrum for the turbulent velocities and energy. Make your estimate in two ways: (a) via dimensional analysis (what quantity can you construct from the energy cascade rate q, atmospheric density ρ and frequency f that has dimensions of pressure?), and (b) via the kinds of arguments about eddy sizes and speeds developed in Sec. 15.4.4.

(b) Your answer in part (i) should scale with frequency as $P(f) \propto 1/f$. In actuality, the measured pressure spectra have a scaling law more nearly like $P(f) \propto 1/f^{2/3}$, not $P(f) \propto 1/f$ [e.g., Fig. 2a of Tanimoto and Um (1999)]. Explain this; i.e., what is wrong with the argument in (i), and how can you correct it to give $P(f) \propto 1/f^{2/3}$? Hint: There is a poem by Lewis Fry Richardson, which says:

> Big whirls have little whirls,
> which feed on their velocity.
> Little whirls have lesser whirls,
> and so on to viscosity.

(c) The low-frequency cutoff for this pressure spectrum is about 0.5 mHz, and at 1 mHz, $P(f)$ has the value $P(f = 1\text{mHz}) \sim 0.3\text{Pa}$, which is about 3×10^{-6} of atmospheric pressure. Assuming that 0.5 mHz corresponds to the largest eddies, which have a length scale of a few km (a little less than the scale height of the atmosphere), derive an estimate for the eddies' turbulent viscosity ν_t in the lower atmosphere. By how many orders of magnitude does this exceed the molecular viscosity? What fraction of the sun's energy input to Earth ($\sim 10^6$ erg cm^{-2} s^{-1}) goes into maintaining this turbulence (assumed to be distributed over the lowermost 10 km of the atmosphere)?

(d) At $f = 1$ mHz, what is the characteristic spatial scale (wavelength) of the relevant normal modes of the Earth? [Hint: The relevant modes have few or no nodes in the radial direction. All you need to answer this is a typical wave speed for seismic shear waves, which you can take to be 5 km/s.] What is the characteristic spatial scale (eddy size) of the atmospheric pressure fluctuations at this same frequency, assuming isotropic turbulence? Suggest a plausible estimate for the rms amplitude of the pressure fluctuation averaged over a surface area equal to one square wavelength of the earth's normal modes. (You must keep in mind the random spatially and temporally fluctuating character of the turbulence.)

(e) Using your answer from (d) and a characteristic shear and bulk modulus for the Earth's deformations of $K \sim \mu \sim 10^{12}$ dyne cm^{-2}, comment on how the observed rms normal-mode acceleration (10^{-10} cm s^{-2}) compares with that expected from stochastic forcing

due to atmospheric turbulence. You may need to go back to Chaps. 11 and 12, and think about the relationship between surface force and surface deformation. [Note: There are several issues in doing this assessment accurately that have not been dealt with in this exercise, e.g. number of modes in a given frequency range; so don't expect to be able to get an answer more accurate than an order of magnitude.]

****

15.5 Turbulent Boundary Layers

Much interest surrounds the projection of spheres of cork, rubber, leather and string by various parts of the human anatomy, with and without the mechanical advantage of levers of willow, ceramic and the finest Kentucky ash. As is well-known, changing the surface texture, orientation, and spin of a ball in various sports can influence the trajectory markedly. Much study has been made of ways to do this both legally and illegally. Some procedures used by professional athletes are pure superstition, but many others find physical explanations that are good examples of the behavior of boundary layers. Many sports involve the motion of balls where the boundary layers can be either laminar or turbulent; his allows opportunities for controlling the flow. With the goal of studying this, let us now consider the structure of a turbulent boundary layer—first along a straight wall, and later along a ball's surface.

15.5.1 Profile of a Turbulent Boundary Layer

In Sec. 14.4.1, we derived the Blasius profile for a laminar boundary layer and showed that its thickness a distance x downstream from the start of the boundary layer was roughly $3\delta = 3(\nu x/V)^{1/2}$, where V is the free-stream speed; cf. Fig. 14.11. As we have described, when the Reynolds number is large enough, $\mathrm{Re}_d = Vd/\nu \sim 3\times 10^5$ or $\mathrm{Re}_\delta \sim \sqrt{\mathrm{Re}_d} \sim 500$ in the case of flow past a cylinder (Figs. 15.1 and 15.2), the boundary layer becomes turbulent.

A turbulent boundary layer consists of a thin *laminar sublayer* of thickness $\delta_{\rm ls}$ close to the wall and a much thicker turbulent zone of thickness δ_t; Fig. 15.10.

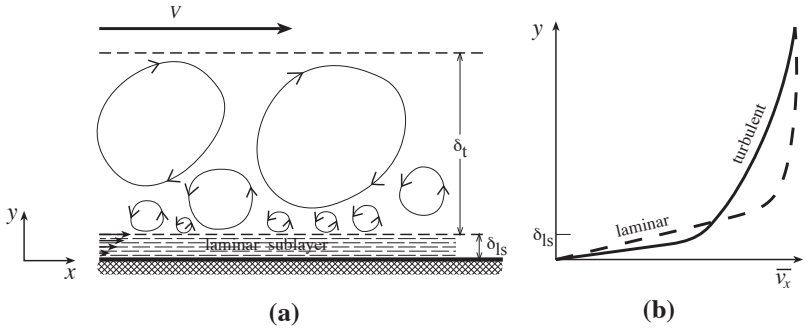

Fig. 15.10: (a) Physical structure of a turbulent boundary layer. (b) Mean flow speed $\mathbf{v}_x$ as a function of distance from the wall for the turbulent boundary layer [solid curve, Eqs. (15.27)] and for a laminar boundary layer [the Blasius profile, Eqs. (14.41)].

In the following paragraphs we shall use the turbulence concepts developed above to compute, in order of magnitude, the structures of the laminar sublayer and the turbulent zone, and the manner in which those structures evolve along the boundary. We denote by y distance perpendicular to the boundary, and by x distance along it in the direction of the flow.

One key to the structure of the boundary layer is the fact that, in the x component of the time-averaged Navier-Stokes equation, the stress-divergence term $T_{xy,y}$ has the *potential* to be so huge (because of the boundary layer's small thickness) that no other term can compensate it. This is true in the turbulent zone, where T_{xy} is the huge Reynolds stress, and also true in the laminar sublayer, where T_{xy} is the huge viscous stress produced by a huge shear that results from the thinness of the layer. (One can check at the end of the following analysis that, for the computed boundary-layer structure, other terms in the x component of the Navier-Stokes equation are indeed so small that they could not compensate a significantly nonzero $T_{xy,y}$.) This *potential* dominance of $T_{xy,y}$ implies that the flow must adjust itself so as to make $T_{xy,y}$ be nearly zero, i.e. T_{xy} be (very nearly) independent of distance y from the boundary.

In the turbulent zone T_{xy} is the Reynolds stress, ρv_ℓ^2, where v_ℓ is the turbulent velocity of the largest eddies at a distance y from the wall; and therefore constancy of T_{xy} implies constancy of v_ℓ. The largest eddies at y will have a size ℓ of order the distance y from the wall, and correspondingly, the turbulent viscosity will be $\nu_t \sim v_\ell y/3$. Equating the expression ρv_ℓ^2 for the Reynolds stress to the alternative expression $2\rho\nu_t \frac{1}{2}\bar{v}_{,y}$ (where $\bar{v}$ is the mean flow speed at y and $\frac{1}{2}\bar{v}_{,y}$ is the shear), and using $\nu_t \sim v_\ell y/3$ for the turbulent viscosity, we discover that in the turbulent zone the mean flow speed varies logarithmically with distance from the wall: $\bar{v} \sim v_\ell \ln y + \text{constant}$. Since the turbulence is created at the inner edge of the turbulent zone, $y \sim \delta_{\rm ls}$, by interaction of the mean flow with the laminar sublayer, the largest turbulent eddies there must have their turnover speeds v_ℓ equal to the mean-flow speed there: $\bar{v} \sim v_\ell$ at $y \sim \delta_{\rm ls}$. This tells us the normalization of the logarithmically varying mean flow speed:

$$\boxed{\bar{v} \sim v_\ell[1 + \ln(y/\delta_{\rm ls})] \quad \text{at } y \gtrsim \delta_{\rm ls}} \,. \tag{15.27a}$$

Turn, next to the structure of the laminar sublayer. There the constant shear stress is viscous, $T_{xy} = \rho\nu\bar{v}_{,y}$. Stress balance at the interface between the laminar sublayer and the turbulent zone requires that this viscous stress be equal to the turbulent zone's ρv_ℓ^2. This equality implies a linear profile for the mean flow velocity in the laminar sublayer, $\bar{v} = (v_\ell^2/\nu)y$. The thickness of the sublayer is then fixed by continuity of $\bar{v}$ at its outer edge, $(v_\ell^2/\nu)\delta_\ell = v_\ell$. Combining these last two relations, we obtain the following profile and laminar-sublayer thickness:

$$\boxed{\bar{v} \sim v_\ell \left(\frac{y}{\delta_{\rm ls}}\right) \quad \text{at } y \lesssim \delta_{\rm ls} \sim \nu/v_\ell} \,. \tag{15.27b}$$

Having deduced the internal structure of the boundary layer, we turn to the issue of what determines the y-independent turbulent velocity v_ℓ of the largest eddies. This v_ℓ is fixed by matching the turbulent zone to the free-streaming region outside it. The free-stream velocity

V must be equal to the mean flow velocity $\bar{v}$ [Eq. (15.27a)] at the outer edge of the turbulent zone. The logarithmic term will dominate, so $V = v_\ell \ln(\delta_t/\delta_{\rm ls})$. Introducing an overall Reynolds number for the boundary layer,

$$\mathrm{Re}_\delta \equiv V\delta_t/\nu, \tag{15.28}$$

and noting that turbulence requires a huge value ($\gtrsim 1000$) of this Re_δ, we can reexpress V as $V \sim v_\ell \ln \mathrm{Re}_\delta$. This should actually be regarded as an equation for the turbulent velocity of the largest scale eddies in terms of the free-stream velocity:

$$\boxed{v_\ell \sim \frac{V}{\ln \mathrm{Re}_\delta}}\,. \tag{15.29}$$

If the thickness δ_t of the entire boundary layer and the free-stream velocity V are given, then Eq. (15.28) determines the boundary layer's Reynolds number, Eq. (15.29) then determines the turbulent velocity, and Eqs. (15.27) determine the layer's internal structure.

Turn, finally, to the issue of how the boundary layer thickness δ_t evolves with distance x down the wall (and correspondingly, how all the rest of the boundary layer's structure, which is fixed by δ_t, evolves). The key to its evolution is *entrainment*, which we met in our discussion of turbulent wakes and jets (Sec. 15.4.3). At the turbulent zone's outer edge, the largest turbulent eddies move with speed $\sim v_\ell$ into the free-streaming fluid, entraining that fluid into themselves Correspondingly, the thickness grows at a rate

$$\boxed{\frac{d\delta_t}{dx} \sim \frac{v_\ell}{V} \sim \frac{1}{\ln \mathrm{Re}_\delta}}\,. \tag{15.30}$$

Since $\ln \mathrm{Re}_\delta$ depends only extremely weakly on δ_t, *the turbulent boundary layer expands essentially linearly with distance x, by contrast with a laminar boundary layer's $\delta \propto x^{1/2}$.*

15.5.2 Coanda Effect and Separation in a Turbulent Boundary Layer

One can easily verify that, not only does the turbulent boundary layer expand more rapidly than the corresponding laminar boundary layer would, if it were stable, but the turbulent layer is also thicker at all locations down the wall. Physically, this can be traced, in part, to the fact that the turbulent boundary layer involves a three-dimensional velocity field, whereas the corresponding laminar layer would involve only a two-dimensional field. The enhanced thickness and expansion contribute to the Coanda effect for a turbulent boundary layer — it's ability to stick to the wall under adverse conditions (Sec. 15.4.3 above).

However, there is a price to be paid for this benefit. Since the velocity gradient is increased close to the surface, the actual surface shear stress exerted by the turbulent layer, through its laminar sublayer, is significantly larger than in the corresponding laminar boundary layer. As a result, if the layer were to remain laminar, the portion that would adhere to the surface would produce less viscous drag than the corresponding portion of the turbulent layer. Correspondingly, in a long, straight pipe, the drag on the pipe wall goes up when the boundary layer becomes turbulent.

However, for flow around a cylinder or other confined body, the drag goes down! cf. Fig. 15.2. The reason is that in the separated, laminar boundary layer the dominant source of drag is not viscosity but rather a pressure differential between the front face of the cylinder, where the layer adheres, and the back face where the reverse eddies circulate. The pressure is much lower in the back-face eddies than in the front-face boundary layer, and that pressure differential gives rise to a significant drag, which gets reduced when the layer goes turbulent and adheres to the back face. Therefore, if one's goal is to reduce the overall drag and the laminar flow is prone to separation, a nonseparating (or delayed-separation) turbulent layer is to be prefered over the laminar layer. Similarly (and for essentially the same reason), for an airplane wing, if one's goal is to maintain a large lift, then a nonseparating (or delayed-separation) turbulent layer is to be prefered over a separating, laminar one.[5]

For this reason, steps are often taken in engineering flows to ensure that boundary layers become and remain turbulent. A crude but effective example is provided by the vortex generators that are installed on the upper surfaces of some airplane wings (Fig. 15.11). These are small obstacles on the wing which penetrate through a laminar boundary layer into the free flow. By changing the pressure distribution, they force air into the boundary layer and initiate three-dimensional vortical motion in the boundary layer forcing it to become

[5]Another example of separation occurs in "Lee waves" which can form when wind blows over a mountain range. These consist of standing-wave eddies in the separated boundary layer, somewhat analogous to the Karman vortex street of Fig. 15.2d; and they are sometimes used by glider pilots to regain altitude.

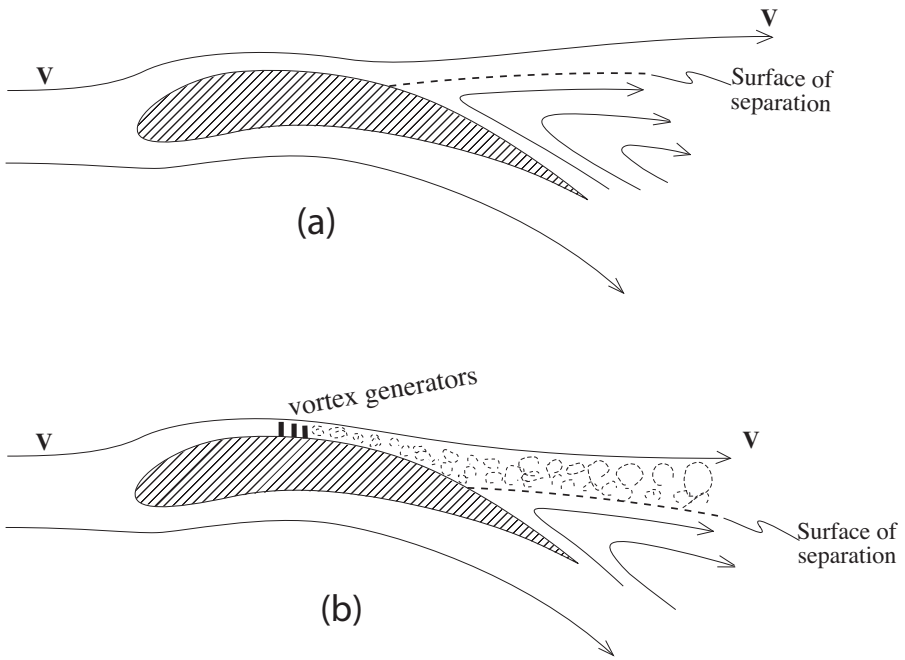

Fig. 15.11: (a) A laminar boundary layer, separating from an airplane wing due to an adverse pressure gradient in the wing's back side. (b) Vortex generators on attached to the wing's top face generate turbulence. The turbulent boundary layer sticks to the wing more effectively than the laminar boundary layer (Coanda effect). Separation from the wing is delayed, and the wing's lift is increased and drag is decreased.

partially turbulent. This can improve the wing's lift, it allows the airplane to climb more steeply without stalling due to boundary-layer separation, and it helps reduce aerodynamical drag.

15.5.3 Instability of a Laminar Boundary Layer

Much work has been done on the linear stability of laminar boundary layers. The principles of such stability analyses should now be familiar, although the technical details are formidable. In the simplest case an equilibrium flow like the Blasius profile is identified and the equations governing the time evolution of small perturbations are written down. The spatial and temporal evolution of individual Fourier components is assumed to vary as $\exp i(\mathbf{k}\cdot\mathbf{x}-\omega t)$, and we seek modes that have zero velocity perturbation on the solid surface past which the fluid flows, and that decay to zero in the free stream. We ask whether there are unstable modes, i.e., modes with real $\mathbf{k}$ for which the imaginary part of ω is positive so they grow exponentially in time. The results can generally be expressed in the form of a diagram like Fig. 15.12.

It is found that there is generally a critical Reynolds number at which one mode becomes unstable. At higher values of the Reynolds number a range of k-vectors are unstable. One interesting result of these calculations is that in the absence of viscous forces (i.e., in the limit $\mathrm{Re}_\delta \to \infty$), the boundary layer is unstable if and only if there is a point of inflection in the velocity profile (a point where d^2v_x/dy^2 changes sign); cf. Fig. 15.12 and Ex. 15.9.

Although, in the absence of an inflection, an inviscid flow $v_x(y)$ is stable, for some such profiles even the slightest viscosity can trigger instability. Physically, this is because viscosity can tap the relative kinetic energies of adjacent flow lines. Viscous-triggered instabilities of this sort are sometimes called *secular instabilities* by contrast with the *dynamical instabilities* that arise in the absence of viscosity. Secular instabilities are quite common in fluid mechanics.

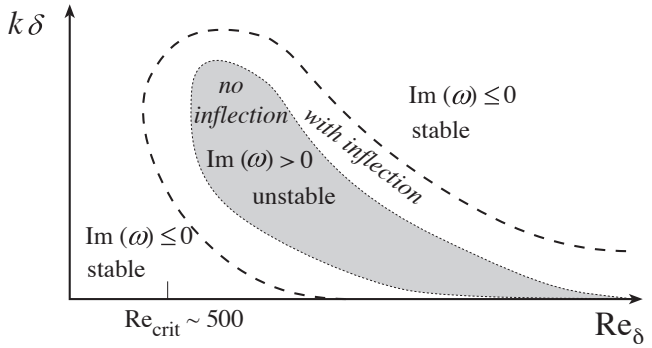

Fig. 15.12: Values of wave number k for stable and unstable wave modes in a laminar boundary layer with thickness δ, as a function of the boundary layer's Reynolds number $\mathrm{Re}_\delta = V\delta/\nu$. If the unperturbed velocity distribution $v_x(y)$ has no inflection point, i.e. if $d^2v_x/dy^2 < 0$ everywhere as is the case for the Blasius profile (Fig. 14.11), then the unstable modes are confined to the shaded region. If there is an inflection point (so $d^2v_x/dy^2 > 0$ near the wall but becomes negative farther from the wall), as is the case near a surface of separation (Fig. 14.12), then the unstable region is larger and does not asymptote to $k = 0$ as $\mathrm{Re}_\delta \to \infty$, i.e. it has a boundary like the dashed curve.

****

EXERCISES

Exercise 15.9 *Problem: Tollmein-Schlicting Waves*
Consider an inviscid ($\nu = 0$), incompressible flow near a plane wall where a boundary layer is established. Introduce coordinates x parallel to the wall and y perpendicular to the wall. Let the components of the equilibrium velocity be $v_x(y)$.

(a) Show that a small perturbation in the velocity, $\delta v_y \propto \exp ik(x - ct)$, with k real and frequency ck possibly complex, satisfies the differential equation

$$\frac{\partial^2 \delta v_y}{\partial y^2} = \left[\frac{1}{(v_x - c)}\frac{d^2 v_x}{dy^2} + k^2\right]\delta v_y \ . \tag{15.31}$$

Hence argue that a sufficient condition for unstable wave modes ($\mathrm{Im}(c) > 0$), is that the velocity field possess a point of inflection; cf. Fig. 15.12. (The boundary layer can also be unstable in the absence of a point of inflection, but viscosity must be present to trigger the instability.)

****

15.5.4 The Flight of a Ball.

Having developed some insights into boundary layers and their stability, we now apply those insights to the balls used in various sports.

The simplest application is to the dimples on a golf ball [Fig. 15.13a]. The dimples provide finite-amplitude disturbances in the flow which can initiate the formation of growing wave modes and turbulence in the boundary layer. The adherence of the boundary layer to the ball is improved and separation occurs further behind the ball leading to a lower drag coefficient and a greater range of flight; see Figs. 15.2 and 15.13a.

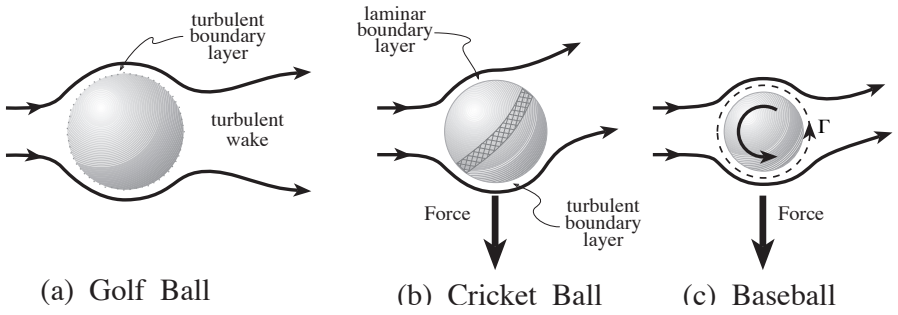

Fig. 15.13: Boundary layers around golf balls, cricket balls, and baseballs, as they move leftward relative to the air — i.e., as the air flows rightward as seen in their rest frames.

A variant on this mechanism is found in the game of cricket, which is played with a ball whose surface is polished leather with a single equatorial seam of rough stitching. When the ball is "bowled" in a non-spinning way with the seam inclined to the direction of motion, there is a laminar boundary layer on the smooth side and a turbulent boundary layer on the side with the rough seam [Fig. 15.13b]. These two boundary layers separate at different points behind the flow leading to a net deflection of the air. The ball will therefore swerve towards the side with the leading seam. (The effect is strongest when the ball is new and still shiny and on days when the humidity is high so the thread in the seam swells and is more efficient at making turbulence.)

This mechanism is different from that used to throw a slider or curveball in baseball, in which the pitcher causes the ball to spin about an axis roughly perpendicular to the direction of motion. In the slider the axis is vertical; for a curveball it is inclined at about 45° to the vertical. The spin of the ball creates circulation (in a nonrotating, inertial frame) like that around an airfoil. The pressure forces associated with this circulation produce a net sideways force in the direction of the baseball's rotational velocity on its leading hemisphere, i.e. as seen by the hitter [Fig. 15.13c]. The physical origin of this effect is actually quite complex and is only properly described with reference to experimental data. The major effect is that separation is delayed on the side of the ball where the rotational velocity is in the same direction as the airflow, and happens sooner on the opposite side [Fig. 15.13c], leading to a pressure differential. The reader may be curious as to how this circulation can be established in view of Kelvin's theorem, Eq. (14.15), which tells us that if we use a circuit that is so far from the ball and its wake that viscous forces cannot cause the vorticity to diffuse to it, then the circulation must be zero. What actually happens is that, when the flow is initiated, starting vortices are shed by the ball and are then convected downstream, leaving behind the net circulation Γ that passes through the ball (Fig. 15.14). This effect is very much larger in two dimensions with a rotating cylinder than in three dimensions because the magnitude of the shed vorticity is much larger. It goes by the name of *Magnus effect* in two dimensions and *Robins effect* in three. It is also useful in understanding the lift in airfoils.

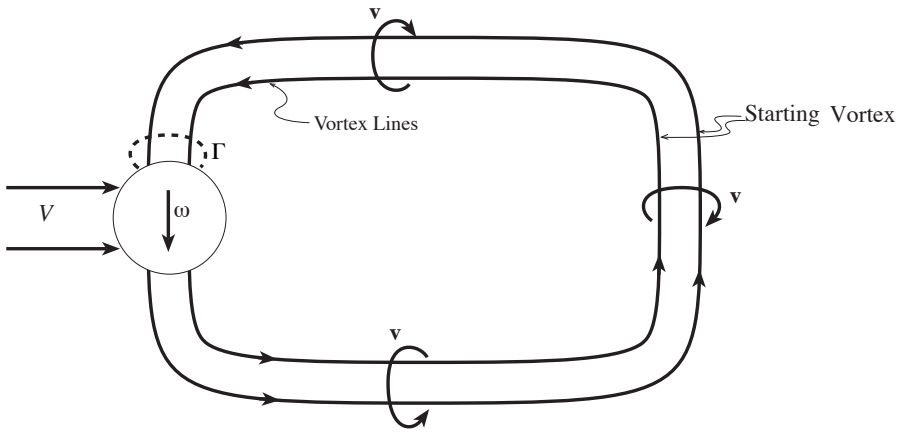

Fig. 15.14: Vortex lines passing through a spinning ball. The starting vortex is created and shed when the ball is thrown, and is carried downstream by the flow as seen in the ball's frame of reference. The vortex lines connecting this starting vortex to the ball lengthen as the flow continues.

In table tennis, a drive is often hit with *topspin* so that the ball rotates about a horizontal axis perpendicular to the direction of motion. In this case, the net force is downwards and the ball falls faster toward the ground, the effect being largest after it has somewhat decelerated. This allows a ball to be hit hard over the net and bounce before passing the end of the table, increasing the margin for errors in the direction of the hit.

Those wishing to improve their curveballs or cure a bad slice are referred to the monographs by Adair (1990), Armenti (1992) and Lighthill (1986).

****

EXERCISES

Exercise 15.10 *Problem: Effect of drag*
A well hit golf ball travels about 300 yards. A fast bowler or fastball pitcher throws a ball at over 90 m.p.h (miles per hour). A table tennis player can hit a forehand return at about 30 m.p.h. The masses and sizes of each of these three types of balls are $m_g \sim 46\text{g}, d_g \sim 43\text{mm}, m_c \sim 160\text{g}, d_c \sim 70\text{mm}, m_b \sim 140\text{g}, d_b \sim 75\text{mm}, m_{tt} \sim 2.5\text{g}, d_{tt} \sim 38\text{mm}$.

(a) For golf, cricket (or baseball) and table tennis, estimate the Reynolds number of the flow and infer the drag coefficient, C_D. (The variation of C_D with Re_d can be assumed to be similar to that in flow past a cylinder.)

(b) Hence estimate the importance of aerodynamic drag in determining the range of a ball in each of these three cases.

****

15.6 The Route to Turbulence: Onset of Chaos

15.6.1 Couette Flow

Let us examine qualitatively how a viscous flow becomes turbulent. A good example is Couette flow between two long, concentric, relatively rotating cylinders as introduced in Sec. 14.6.4 and depicted in Fig. 15.15a. The Rayleigh stability criterion (flow unstable if and only if angular momentum per unit mass decreases outward) was derived in Sec. 14.6.4 ignoring viscous stress. Now suppose we have a flow that is stable according to the Rayleigh criterion. Suppose, further, that the fluid is a liquid and we steadily decrease its viscosity by heating it, so the Reynolds number steadily increases. At low Re, the equilibrium flow is stationary and azimuthal [strictly in the ϕ direction in Fig. 15.15a]. However, at some critical Reynolds number Re_{c1}, the flow becomes unstable to the growth of small perturbations, and these perturbations drive a transition to a new, stationary equilibrium that involves poloidal circulation (quasi-circular motions in the r and z directions, called *Taylor rolls*); see Fig. 15.15a.

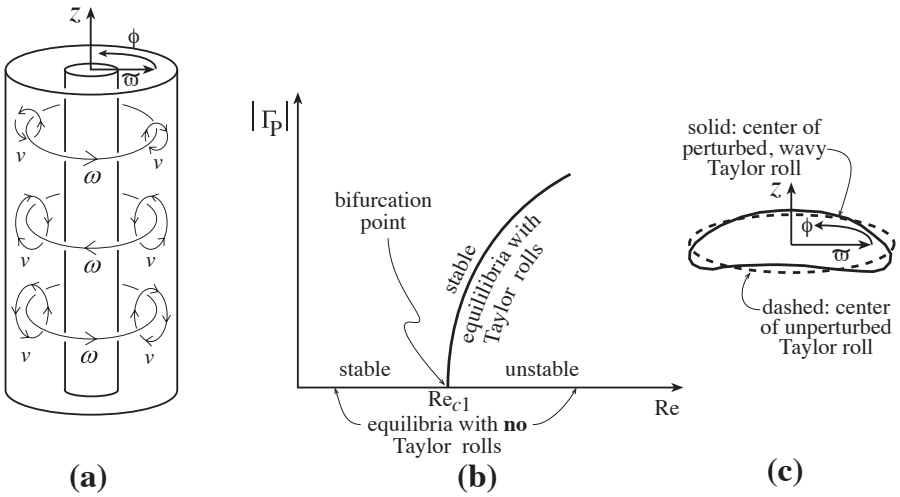

Fig. 15.15: Bifurcation in Couette flow. (a) Equilibrium flow with Taylor rolls. (b)Bifurcation diagram in which the amplitude of the poloidal circulation $|\Gamma_{\rm P}|$ in a Taylor roll is plotted against the Reynolds number Re. At low Re ($\mathrm{Re} < \mathrm{Re}_{c1}$) the only equilibrium flow configuration is smooth, azimuthal flow. At larger Re ($\mathrm{Re}_{c1} < \mathrm{Re} < \mathrm{Re}_{c2}$) there are two equilibria, one with Taylor rolls and stable, the other the smooth, azimuthal flow, which has become unstable. (c) Shape of a Taylor roll at $\mathrm{Re}_{c1} < \mathrm{Re} < \mathrm{Re}_{c2}$ (dashed ellipse) and at higher Re, $\mathrm{Re}_{c2} < \mathrm{Re} < \mathrm{Re}_{c3}$ (wavy curve).

What has happened is that an equilibrium with a high degree of symmetry has become unstable, and a new, lower-symmetry, stable stable equilibrium has taken over; see Fig. 15.15b. Translational invariance along the cylinder axis has been lost from the flow, despite the fact that the boundary conditions remain translationally symmetric. This change of equilibrium mode is another example of a bifurcation like that discussed when we treated the buckling of beams and playing cards (Secs. 11.8 and 12.3.5).

As Re is increased further, this process repeats: At a second critical Reynolds number Re_{c2}, there is a second bifurcation of equilibria in which the azimuthally smooth Taylor rolls become unstable and are replaced by new, azimuthally wavy Taylor rolls; see Fig. 15.15c. Again, an equilibrium with higher symmetry (rotation invariance) has been replaced, at a bifurcation point, by one of lower symmetry (no rotation invariance). There is a fundamental frequency f_1 associated with the wavy Taylor rolls' motion as they circulate around the central cylinder. Since the waves are nonlinearly large, harmonics of this fundamental are also seen when one Fourier decomposes the velocity field; cf. Fig. 15.16a. When Re is increased still further to some third critical value Re_{c3}, there is yet another bifurcation. The Taylor rolls now develop a second set of waves, superimposed on the first, with a corresponding new fundamental frequency f_2 that is incommensurate with f_1. In the energy spectrum one now sees various harmonics of f_1 and of f_2, as well as sums and differences of these two fundamentals; cf. Fig. 15.16b.

It is exceedingly difficult to construct experimental apparatus that is clean enough, and free enough from the effects of finite lengths of the cylinders, to reveal what happens next as one turns up the Reynolds number. However, despite the absence of clean experiments, it seemed obvious before the 1970's what would happen: The sequence of bifurcations would

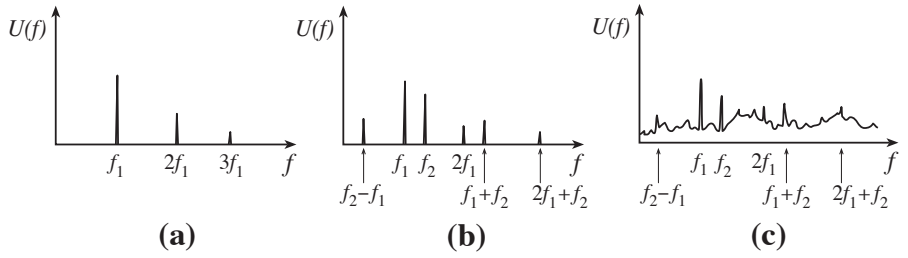

Fig. 15.16: The energy spectrum of velocity fluctuations in rotating Couette flow (schematic). (a) For a moderate Reynolds number, $\mathrm{Re}_{c2} < \mathrm{Re} < \mathrm{Re}_{c3}$, at which the stable equilibrium flow is that with the wavy Taylor rolls of Fig. 15.15c. (b) For a higher Reynolds number, $\mathrm{Re}_{c3} < \mathrm{Re} < \mathrm{Re}_{c4}$, at which the stable flow has wavy Taylor rolls with two incommensurate fundamental frequencies present. (c) For a still higher Reynolds number, $\mathrm{Re} > \mathrm{Re}_{c4}$, at which turbulence has set in.

continue, with ever decreasing intervals of Reynolds number $\Delta\mathrm{Re}$ between them, producing after awhile such a complex maze of frequencies, harmonics, sums, and differences, as to be interpreted as turbulence. Indeed, one finds the onset of turbulence described in just this manner in the classic fluid mechanics textbook of Landau and Lifshitz (1959).

The 1970's and 1980's brought a major breakthrough in our understanding of the onset of turbulence. This breakthrough came from studies of model dynamical systems with only a few degrees of freedom, in which nonlinear effects play similar roles to the nonlinearities of the Navier-Stokes equation. These studies revealed only a handful of routes to irregular or unpredictable behavior known as chaos, and none were of the Landau-Lifshitz type. However, one of these routes starts out in the same manner as does rotating Couette flow: As a control parameter (Reynolds number for Couette flow) is gradually increased, first oscillations with one fundamental frequency f_1 and its harmonics turn on; then a second frequency f_2 and its harmonics turn on, along with sums and differences of f_1 and f_2; and then, suddenly, chaos sets in. Moreover, the chaos is clearly not being produced by a complicated superposition of other, new frequencies; it is fundamentally different from that. The best Couette-flow experiments of the 1980's and later appear to confirm that the onset of turbulence goes by this route; see Fig. 15.16c.

15.6.2 Feigenbaum Sequence and Onset of Turbulence in Convection

The very simplest of systems in which one can study the several possible routes to chaos are one-dimensional mathematical maps. A lovely example is the "Feigenbaum sequence," explored by Mitchell Feigenbaum in the 1970's.

The Feigenbaum sequence is a sequence $\{x_1, x_2, x_3, \ldots\}$ of values of a real variable x,

given by the rule (sometimes called the *logistic equation*) [6]

$$x_{n+1} = 4ax_n(1 - x_n). \tag{15.32}$$

Here a is a fixed "control" parameter. It is easy to compute Feigenbaum sequences $\{x_n\}$ for different values of a on a personal computer (Ex. 15.11). What is found is that there are critical parameters $a_1, a_2, \ldots$ at which the character of the sequence changes sharply. For $a < a_1$, the sequence asymptotes to a stable fixed point. For $a_1 < a < a_2$, the sequence asymptotes to stable, periodic oscillations between two fixed points. If we increase the parameter further, so that $a_2 < a < a_3$, the sequence becomes a periodic oscillation between four fixed points. The period of the oscillation has doubled. This *period doubling* (NOT frequency doubling) happens again: When $a_3 < a < a_4$, x asymptotes to regular motion between eight fixed points. Period doubling increases with shorter and shorter intervals of a until at some value a_∞, the period becomes infinite and the sequence does not repeat. Chaos has set in.

This period doubling is a second route to chaos, very different in character from the "one-frequency, two-frequencies, chaos" route that one meets in Couette flow. Remarkably, fluid dynamical turbulence can set in by this second route, as well as by the first. It does so in certain very clean experiments on convection in liquid helium. We shall return to this below, and then again in Sec. 16.6.

How can so starkly simple and discrete a thing as a one-dimensional map bear any relationship at all to the continuous solutions of the fluid dynamical differential equations? The answer is quite remarkable:

Consider a steady flow in which one parameter a (e.g. the Reynolds number) can be adjusted. Now, as we change a and approach turbulence, the flow may develop a periodic oscillation with a single frequency f_1. We could measure this by inserting some probe at a fixed point in the flow to measure a fluid variable y, e.g. one component of the velocity. We can detect the periodicity either by inspecting the readout $y(t)$ or its Fourier transform $\tilde{y}$. However, there is another way, that may be familiar from classical mechanics. This is to regard $\{y, \dot{y}\}$ as the two coordinates of a two-dimensional phase space. (Of course, instead one could measure many variables and their time derivatives, resulting in an arbitrarily large phase space, but let us keep matters as simple as possible.) For a single periodic oscillation, the system will follow a closed path in this phase space [Fig. 15.17a]. As we increase a further, a period doubling may occur and the trajectory in phase space may look like Fig. 15.17b. Now, as we are primarily interested in the development of the oscillations, we need only keep one number for every fundamental period $P_1 = 1/f_1$. Let us do this by taking a section through phase space and introducing a coordinate x on this section as shown in Fig. 15.17. The n'th time the trajectory crosses through this section, its crossing point is x_n, and the mapping from x_n to x_{n+1} can be taken as a representative characterization of the flow. When only the frequency f_1 is present, the map will read $x_{n+2} = x_n$ [Fig. 15.17a]. When f_1 and $f_2 = \frac{1}{2}f_1$ are present, the map will read $x_{n+4} = x_n$ [Fig. 15.17b]. (These specific maps are

[6] This equation first appeared in discussions of population biology (Verhulst, 1838). If we consider x_n as being proportional to the number of animals in a species, the number in the next season should be proportional to the number of animals already present and to the availability of resources which will decrease as x_n approaches some maximum value, in this case unity. Hence the terms x_n and $1 - x_n$ in Eq. (15.32).

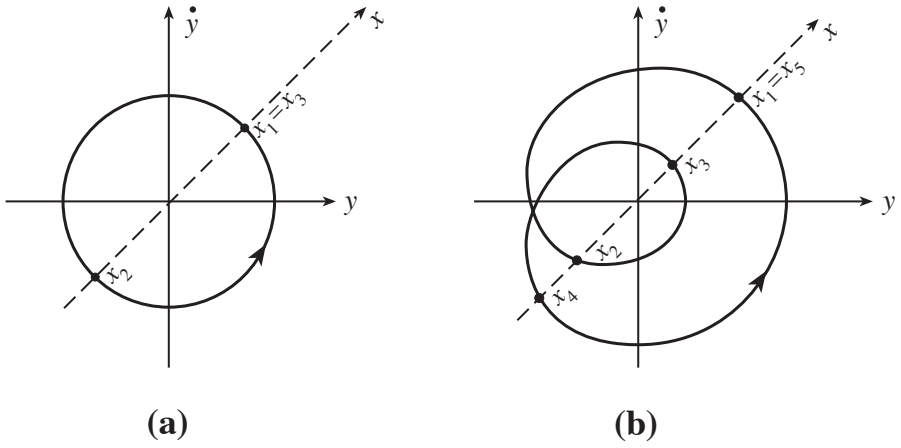

Fig. 15.17: a) Representation of a single periodic oscillation as motion in phase space. b) Motion in phase space after period doubling. The behavior of the system may also be described by using the coordinate x of the Poincaré map.

overly simple compared to what one may encounter in a real flow, but they illustrate the idea.)

To reiterate, instead of describing the flow by the full solution $\mathbf{v}(\mathbf{x}, t)$ to the Navier-Stokes equations and the flow's boundary conditions, we can construct the simple map $x_n \rightarrow x_{n+1}$ to characterize the flow. This procedure is known as a *Poincaré map*. The mountains have labored and brought forth a mouse! However, this mouse turns out to be all that we need. For some convection experiments, just the same period doubling behavior and approach to chaos are present in these maps as in the two-dimensional phase-space diagram and in the full solution to the fluid dynamical equations; and when observed in the Poincaré maps, it looks qualitatively the same as in the Feigenbaum sequence. It is remarkable that for a system with so many degrees of freedom, chaotic behavior can be observed by suppressing almost all of them.

If, in the period-doubling route to chaos, we compute the limiting ratio of successive critical parameters,

$$\mathcal{F} = \lim_{j\rightarrow\infty} \frac{a_j - a_{j-1}}{a_{j+1} - a_j}, \tag{15.33}$$

we find that it has the value $4.6692016090\ldots$. This (Feigenbaum) number seems to be a universal constant characteristic of most period doubling routes to chaos, independent of the particular map that was used. For example, if we had used

$$x_{n+1} = a \sin \pi x_n \tag{15.34}$$

we would have got the same constant.

The most famous illustration of the period doubling route to chaos is a classic experiment by Libchaber and Maurer (1978) on convection in liquid helium. The temperature at a point was monitored with time as the helium's vertical temperature gradient was slowly increased. Initially, the temperature was found to oscillate with a single period, but then subharmonics started appearing one after another, until, eventually, the flow became turbulent. Libchaber

was able to measure the ratio (15.33) accurate to about 3 per cent (with a_j the temperature at which the j'th period doubling occurred). His result agreed with Feigenbaum's number to within his experimental accuracy!

For several other routes to chaos identified in convection experiments, see Gollub and Benson (1980).

When chaos sets in, the evolution of the system becomes essentially incalculable. This is because, as can be shown mathematically, the future state, as measured by the values of a set of fluid variables at some subsequent time (or by the value of a map), becomes highly sensitive to the assumed initial conditions. Paths in phase space (or in the mapping) that start extremely close to one another diverge from each other exponentially rapidly with time.

It is important to distinguish the unpredictability of classical chaos from unpredictability in the evolution of a quantum mechanical system. A classical system evolves under precisely deterministic differential equations. Given a full characterization of the system at any time t, the system is fully specified at a later time $t+\Delta t$, for any Δt. However, what characterizes a chaotic system is that the evolution of two identical systems in neighboring initial states will eventually evolve so that they follow totally different histories. The time for this to happen is called the Lyapunov time. The practical significance of this essentially mathematical feature is that if, as will always be the case, we can only specify the initial state up to a given accuracy (due to practical considerations, not issues of principle), then the true initial state could be any one of those lying in some region, so we have no way of predicting what the state will be after a few Lyapunov times. Quantum mechanical indeterminacy is different. If we can prepare a system in a given state described by a wave function, then the wave function's evolution will be governed fully deterministically by the time-dependent Schrödinger equation. However, if we choose to make a measurement of an observable, many quite distinct outcomes are immediately possible and the system will be left in an eigenstate corresponding to the actual measured outcome. The quantum mechanical description of classical chaos is the subject of quantum chaos.

The realisation that many classical systems have an intrinsic unpredictability despite being deterministic from instant to instant has been widely publicised in popularisations of research into chaos. However it is not particularly new. It was well understood, for example, by Poincaré around 1900, and watching the weather report on the nightly news bears witness to its dissemination into the popular culture! What *is* new and intriguing is the manner in which the transition from a deterministic to a non-predictable evolution happens.

Chaotic behavior is well documented in a variety of physical dynamical systems: electrical circuits, nonlinear pendula, dripping faucets, planetary motions and so on. The extent to which the principles that have been devised to describe chaos in these systems can also be applied to general fluid turbulence remains a matter for debate. There is no question that there are similarities, and there has been quantitative success in applying chaos results to a limited form of turbulent convection. However, most forms of turbulence are not so easily described and there is still a huge gap between the intriguing mathematics of chaotic dynamics and practical applications to natural and technological flows.

****

EXERCISES

Exercise 15.11 *Problem: Feigenbaum Sequence*
Use a computer to calculate the first five critical parameters a_j in the Feigenbaum sequence, Eq. (15.32). Hence verify that the ratio of successive differences, tends toward the limit quoted in Eq. (15.33). (Hint. You might find it helpful to construct a graph to find suitable starting values, x_1 and starting parameters a.)

Exercise 15.12 *Example: Lyapunov Exponent*
Consider the logistic equation (15.32) for the special case $a = 1$, which is large enough to ensure that chaos has set in.

(a) Make the substitution $x_n = \sin^2 \pi\theta_n$ and show that the equation can be expressed in the form $\theta_{n+1} = 2\theta_n (\text{mod } 1)$; i.e., $\theta_{n+1} =$ fractional part of $2\theta_n$. .

(b) Write θ_n as a "binimal" (binary decimal). For example $11/16 = 1/2 + 1/8 + 1/16$ has the binary decimal form 0.1011 . Explain what happens to this number in each successive iteration.

(c) Now suppose that an error is made in the i'th digit of the starting binimal. When will it cause a major error in the predicted value of x_n?

(d) If the error after n iterations is written ϵ_n, show that the Lyapunov exponent p defined by

$$p = \lim_{n\to\infty} \frac{1}{n} \ln \left| \frac{\epsilon_n}{\epsilon_0} \right| \tag{15.35}$$

is $\ln 2$ (so $\epsilon_n \simeq 2^n \epsilon_0$ for large enough n). Lyapunov exponents play an important role in the theory of dynamical systems.

Exercise 15.13 *Example: Strange Attractors*
Another interesting one-dimensional map is provided by the recursion relation,

$$x_{n+1} = a\left(1 - 2\left|x_n - \frac{1}{2}\right|\right) \tag{15.36}$$

(a) Consider the asymptotic behavior of the variable x_n for different values of the parameter a, with both x_n and a being confined to the interval $[0, 1]$. In particular find that for $0 < a < a_{\text{crit}}$ (for some a_{crit}), the sequence x_n converges to a stable fixed point, but for $a_{\text{crit}} < a < 1$, the sequence wanders chaotically through some interval $[x_{\min}, x_{\max}]$.

(b) Using a computer, calculate the value of a_{crit} and the interval $[x_{\min}, x_{\max}]$ for $a = 0.8$.

(c) The interval $[x_{\min}, x_{\max}]$ is an example of a *strange attractor*. It has the property that if we consider sequences with arbitrarily close starting values, their values of x_n in this range will eventually diverge. Show that the attractor is strange by computing the sequences with $a = 0.8$ and starting values $x_1 = 0.5, 0.51, 0.501, 0.5001$. Determine

the number of iterations n_ϵ required to produce significiant divergence as a function of $\epsilon = x_1 - 0.5$. It is claimed that $n_\epsilon \sim -\ln_2(\epsilon)$. Can you verify this? Note that the onset of chaos at $a = a_{\rm crit}$ is quite sudden in this case, unlike the behavior exhibited by the Feigenbaum sequence.

Exercise 15.14 *Problem: Lorenz Equations*
One of the first discoveries of chaos in a mathematical model was by Lorenz (1963), who made a simple model of atmospheric convection. In this model, the temperature and velocity field are characterized by three variables, x, y, z, which satisfy the coupled, nonlinear differential equations

$$\begin{aligned} dx/dt &= 10(y - x) \ , \\ dy/dt &= -xz + 28x - y \ , \\ dz/dt &= xy - 8z/3 \ . \end{aligned} \tag{15.37}$$

(The precise definitions of x, y, z need not concern us here.) Integrate these equations numerically to show that x, y, z follow non-repeating orbits in the three-dimensional phase space that they span, but follow certain broadly defined paths in this space. (It may be helpful to plot out the trajectories of pairs of the dependent variables.)
[Note: These Lorenz equations are often studied with the numbers 10, 28, 8/3 replaced by parameters σ, ρ, and β. As these parameters are varied, the behavior of the system changes.]

****

Bibliographic Note

Turbulence is omitted from many standard textbooks on fluid mechanics, aside from brief descriptions, presumably because it is so poorly understood. Good textbook treatments can be found in White (1991), Tennekes and Lumley (1972), and from a more physical perspective, Tritton (1977). To develop physical insight into turbulence, we recommend viewing the movies by Stewart (1968) and Rouse (1963) and looking at photographs, e.g. in Van Dyke (1982). For the influence of boundary layers and turbulence on the flight of balls of various sorts, see Adair (1990), Armenti (1992), and Lighthill (1986). For the onset of turbulence, and more generally the onset of chaos in dynamical systems and mathematical maps, see Sagdeev, Usikov and Zaslavsky (1988), and Acheson (1990).

Bibliography

Acheson, D. J. 1990. *Elementary Fluid Dynamics*, Oxford: Clarendon Press.

Box 15.4
Important Concepts in Chapter 15

- Weak turbulence contrasted with strong or fully developed turbulence, Sec. 15.1
- Scaling relation, Sec. 15.2
- Stagnation pressure, Sec. 15.2
- Drag coefficient, Sec. 15.2
- Karman vortex street, Sec. 15.2
- Critical Reynolds number, $\mathrm{Re}_d \sim 1000$, for onset of turbulence, Sec. 15.2
- Entrainment, Coanda effect, and its role on airplane wings, Secs. 15.2, 15.5.1, Ex. 15.7
- Intermittency, Sec. 15.1
- Role of vorticity in turbulence: stretching of vortex tubes, Sec. 15.3.1, Fig. 15.5
- Eddies, energy cascade, viscous damping at smallest scale, Sec. 15.4.4
- Kolmogorov spectrum, Sec. 15.4.4
- Weak turbulence theory, Sec. 15.4
  - Decomposition into time averaged flow and fluctuating flow, Sec. 15.4.1
  - Reynolds stress, tubulent viscosity, and their role in coupling fluctuating flow to time-averaged flow, Secs. 15.4.1, 15.4.2
  - The physics that governs the structure of the time-averaged flow in boundary layers, wakes and jets, Sec. 15.5.1, Exs. 15.5, 15.6
- Secular instability contrasted with dynamical instability, Sec. 15.5.3
- Rotating Couette flow, Sec. 15.6.1
- Poincaré map and its use to produce discrete maps that characterize a flow, Sec. 15.6.2
- Lyapunov exponent, Ex. 15.12
- Strange attractor, Ex. 115.13

Adair, R. K. 1990. *The Physics of Baseball*, New York: Harper and Row.

Armenti, A., Jr., editor 1992. *The Physics of Sports*, New York: The American Institute of Physics.

Drazin, P. G. and Reid, W. H. 1981. *Hydrodynamic Stability*, Cambridge: Cambridge University Press.

Feigenbaum, M. 1978. "Universal behavior in nonlinear systems," *J. Stat. Phys.*, **19**, 25.

Gollub, J. P. 1980. "Many routes to turbulent convection," *J. Fluid. Mech.*, **100**, 449.

Landau, L. D. and Lifshitz, E. M. 1959. *Fluid Mechanics*, Reading, Massachusetts: Addison Wesley.

Libchaber, A. and Maurer, J. "Local probe in a Rayleigh-Bénard expriment in liquid helium," *Phys. Lett. Paris,* **39**, L369 (1978).

Lighthill, M. J. 1986. *An Informal Introduction to Theoretical Fluid Mechanics*, Oxford: Oxford Science Publications.

Lorenz, E. N. 1963. "Deterministic nonperiodic flow". *J. Atmospheric Sciences*, **20**, 130.

Ott, E. 1982. "Strange attractors and chaotic motions of dynamical systems" *Rev. Mod. Phys.*, **53**, 655.

Ott, E. 1993. *Chaos in Dynamical Systems*, Cambridge: Cambridge University press.

Rouse, H. 1963. *Laminar and Turbulent Flow*, a movie; available in 2012 at `http://www.iihr.uiowa.edu/research/publications-and-media/films-by-hunter-rouse/` .

Sagdeev, R. Z., Usikov, D. A., and Zaslovsky, G. M. 1988. *Non-Linear Physics from the Pendulum to Turbulence and Chaos*, Harwood.

Stewart, R. W. 1968. *Turbulence*, a movie (National Committee for Fluid Mechanics Films); available at http://web.mit.edu/fluids/www/Shapiro/ncfmf.html .

Tanimoto, T. and Um, J. 1999. "Cause of Continuous Oscillations of the Earth," *J. Geophysical Research*, **104**, No. B12, pp. 28723–28739.

Tennekes, H. and Lumley, J. L. 1972. *A First Course on Turbulence*, Cambridge: MIT Press.

Tritton, D. J. 1977. *Physical Fluid Dynamics*, New York: Van Nostrand Reinhold.

Van Dyke, M. 1982. *An Album of Fluid Flow*, Stanford: Parabolic Press.

Verhulst, P. F. 1838. "Notice sur la loi que la population poursuit dans son accroissement," *Correspondance Mathématique et Physique* **10**, 113.

White, F. M. 1991. *Viscous Fluid Flow*, second edition, New York: McGraw Hill.